

Department of Mechanical Engineering

**Design of a Prototype Hybrid Electrical Serial
Drive System for Motor
Vehicular Applications**

Author:

John Egbuta

Supervisor:

Dr. Nick Kelly

A thesis submitted in partial fulfilment for the requirement of degree in
Master of Science in Energy Systems and the Environment

2009

Copyright Declaration

This thesis is the result of the author's original research. It has been composed by the author and has not been previously submitted for examination which has led to the award of a degree.

The copyright of this thesis belongs to the author under the terms of the United Kingdom Copyright Acts as qualified by University of Strathclyde Regulation 3.50. Due acknowledgement must always be made of the use of any material contained in, or derived from, this thesis.

Signed: John Egbuta

Date: 18th September 2009

Abstract

The term Hybrid Vehicle as defined by the United Nations is a vehicle with 2 different energy converters and 2 different energy storage systems for the purpose of propulsion. The Hybridization of renewable energy sources to create cleaner and more efficient solutions for vehicular transport has led to the design of various modular technologies in which the traditional Internal Combustion Engine (ICE) driven by petrol is combined with an alternative energy source in the drive train. Hybrid designs exist, such as the Serial, Parallel, Combined, through the road, Two Mode, Micro and Mild, Full and Plug in Hybrids.

In this thesis, a prototype of the serial hybrid electric drive was designed to investigate the capability of combining a Hydrogen fuel cell and Lithium Ion Battery Power Pack to power a DC Motor using an embedded MSP430 Micro controller to digitally control the Battery charging program. Basically, the system is a standalone battery charger combined with a DC motor, in which the DC motor is driven only by the Li-Ion Battery Pack while it is charged by the Hydrogen Fuel Cell. This hybrid electric drive system was designed at the Greenspace Research-Hydrogen Labs using the Heliocentris FC-50 PEM Fuel Cell to provide power to charge the Li-Ion Battery.

A complete analysis of the loading effect of the DC motor on the battery pack was done as observations were made on the charge and discharge states. An investigation into the variation of the DC motor speeds over a period of time (also known as a Drive Cycle) was executed. These Drive cycles were also generated to understand the impact of starts and stops as well as the impact of the charging program on the battery over a period of time, as a steady energy source is dissipated as it drives a load. Since this is a Prototypical Drive System, the basic properties of the drive train were measured and analyzed, such as the Mechanical Power, Torque, Motor Speeds, Efficiency and Loading effect on the motor as drive cycles were emulated.

The specific objective of this work is therefore to verify the efficacy of the embedded MSP430 microcontroller to digitally control the charge program for the Li-Ion Battery pack when the DC motor is mobile and stationary and provide peak power directly

from the Li-Ion Battery pack (while it is charged by the PEM Fuel Cell) as it drives the motor over a specified time period.

The next 4 sections of this thesis will cover the literature review of the current hybrid electric drive systems and more importantly the current serial drive systems available and prototypes in the market; this will be followed by methods and materials, which is the storyline of the research endeavour at the hydrogen labs at Greenspace Research involving the design, build and test phases of the different modules of this prototype; followed by Results and Discussion of the data acquired by the National Instruments Labview Signal Express Program and tachometer measurements of varying speeds over the different drive cycles as well as the analysis of this data; Finally, conclusions will be made and recommendations regarding future improvements on this prototype will be proposed.

Acknowledgements

I would like to express my gratitude to Greenspace Research, UK for providing the quintessential environment to conduct research on the design of this prototype. Special Mention has to be made of Dr. Alasdair Macleod and the aids he provided during the course of the deployment of the Heliocentris Instructor and the rest of the team at Greenspace Research who provided all the components for this project. Without them, this prototype would not have been designed.

I also want to thank the Comhairle nan Eilean Siar for making the placement at Greenspace Research possible. I am thankful for the direction for research provided by the Royal Mail Bus Service.

I also want to thank Dr. Nick Kelly for providing guidance during the course of this project.

Lastly, I am thankful to God for my family who stood with me through the course of the MSc. Program and supported me, may God Bless you all.

Table of Contents

Chapter 1.0	Introduction.....	10
Chapter 2.0	Literature Review.....	14
2.1.	PEM Fuel Cell.....	15
2.1.1.	Heliocentris FC50.....	16
2.2	Lithium Ion Batteries.....	17
2.2.1	Origins	17
2.2.2	Advantages.....	17
2.2.3	Disadvantages.....	18
2.2.4	Charging the Li-Ion battery.....	18
2.2.5	Varta Li-Ion Battery Design.....	19
2.3	Direct Current Motors.....	22
2.3.1	Description	22
2.3.2	Mechanical Power.....	23
2.3.3	Mechanical Torque.....	24
2.3.4	Speed of Rotation.....	24
2.3.5	Efficiency.....	24
2.4	Electric Drive Technologies.....	25
2.4.1	Electric Drive Hybridisation.....	26
2.4.2	Serial Hybrid Drives	26
2.4.3	Parallel Hybrid Drives.....	27
2.4.4	Combined Hybrid Drives.....	28

2.5	MSP430F2132 Mixed Signal Micro-controller.....	30
2.5.1	Description.....	30
2.5.2	Operating Modes.....	33
2.5.3	Digital Input / Output.....	34
2.5.1d	Timers.....	34
2.5.1e	Analogue to Digital Converters.....	35
Chapter 3.0	Methods and Materials.....	36
3.1	System Architecture and Modular Design	37
3.1.1	MSP430 Microcontroller Programme Design Environment...41	
3.1.1a	Charge Control Algorithm	42
3.1.1b	Source code Design, Build and Test.....	48
3.2	Full System Integration	49
3.2.1	Design, Build of Test System with Dual Power Supply Unit.49	
3.2.2	Integration of Stand Alone System.....	51
3.3	Drive Cycle Emulation and Motor Load Design.....	53
Chapter 4.0	Results and Discussions.....	54
4.1	Charge Cycle Analysis.....	54
4.2	Discharge Cycle Analysis.....	57
4.3	Drive Cycle Analysis	62
4.4	DC Motor Characteristics during Drive Cycle Emulation....	65
Chapter 5.0	Conclusions and Recommendations.....	67
5.1	Conclusions.....	67

5.2	Recommendations.....	68
5.3	Limitations.....	68
	References.....	70
	Appendices	

List of figures

Figure 1 Brent Crude Oil Prices per Barrel (courtesy thisismoney.co.uk)

Figure 2 PEM Fuel Cell

Figure 3. The Heliocentris Instructor

Figure 4. Constant Voltage Charge program for a 3.7V Lithium Ion Battery

Figure 5a Basic Principle of the Lithium Ion Battery

Figure 5b Varta Lithium ion battery with Protection Circuit Module

Figure 6 CEMF in a DC motor

Figure 7 Serial Hybridization of Battery and ICE Power trains

Figure 8 Parallel Hybridization of the ICE and battery powertrains

Figure 9 Series-parallel or combined hybridization

Figure 10 Planetary Gear System: T and Omega represent Torques and Correspondent speeds in the electric motors and the different components of the planetary gear unit.

Figure 11 I/O Pins

Figure 12 MSP430 CPU Architecture

Figure 13 Operating Modes of the MSP430F2132

Figure 14 Timer A

Figure 16 10bit ADC

Figure 17a Schematic of the Hybrid Electric Serial Drive

Figure 17b Block Diagram of Hybrid Electrical Serial Drive System (aka volTRONe)

Figure 18 Data Acquisition Module

Figure 19 NI-Signal Express Data Playback of charge program.

Figure 20 Voltage Regulation Module.

Figure 20a Battery Charger Block diagram

Figure 20b Flowchart showing the charge algorithm

Figure 20c Battery charger source code

Figure 21 Pulse Width Modulation of Li-Ion battery voltage.

Figure 22 Source Code Modular Design Process

Figure 23 Initial Test Module with Dual Power Supply Unit and Oscilloscope

Figure 24. Dual Power Supply and Initial circuitry showing the Power Supply and Pulse width Modulation Test Modules

Figure 25 Fully Integrated Standalone system

Figure 26 The Drive Cycle Emulator

Figure 27 Stornoway-Port Ness Route

Figure 28 Charge cycle of the battery

Figure 29 Voltage of the Li-Ion Battery during the constant voltage charge cycle

Figure 30 FC 50 voltage data during charge cycle

Figure 31 Discharge cycle of the battery showing FC50 and Battery voltages

Figure 32 Voltage of the Li-ion battery during charge cycle

Figure 33 Initial loading of the battery to emulate sloped terrain

Figure 34 Over-discharge of the battery and protection circuit activation

Figure 35 Short Stop and recharge

Figure 36 Final discharge and end of drive cycle

Figure 37 Delay/Resume sequence for final discharge.

Figure 38 Western Isles map and red route

Figure 39 Drive Cycle Emulation for the journey from Port Ness to Stornoway

Figure 40 Discharge cycle of battery during Drive Cycle emulation shown in figure 39

Figure 41 Short Stop at Bavrás (region C of drive cycle)

Figure 42 Current data for 1.2ohm resistor (current values were divided by 1000)

1.0 Introduction

The first decade of the 21st century saw the crash of crude oil prices as it spiralled from a peak of 144.95 USD to 38.12 USD (i.e. Brent Crude, see figure 1). All this happening within a period of 6 months, when there were speculations of even higher prices and the ushering in of an era of economical growth for the Developing economies in the far East and abroad.



Figure 1 Brent Crude Oil Prices per Barrel [1]

In the movie, *A Crude Awakening-The Oil Crash* [2], Energy Analysts and major players in the Oil Industry such as Matthew Simmons, Dr. Colin Campbell (author of *The Coming Oil Crisis*) and Terry Lynn Karl support the theory that, we are moving from an era of cheap abundant energy to an era of scarce hard to get expensive energy, while at the same time making ourselves dependent on some extremely unstable regimes in some nasty parts of the world.

According to Dr. Colin Campbell, the crude oil reserves that were formed briefly over geological time have been used up over 2 centuries. The fact that oil reserves today are

questionable in terms of meeting the needs of the demand of developing countries like China and India leads to an inescapable reality, that Energy Supply from Crude Oil is no longer sustainable and we can no longer continue to rely solely on this source of energy. The last major oil discoveries occurred between 1967-1969 in the Alaskan North Slope, Siberia, Siberia and the North Sea. Since then, most of the major crude oil producing nations have peaked and are producing significantly less than they did 3 decades ago.

Transport forms a huge component of the demand for crude oil and the threat of unsustainable crude oil supplies has led to the Hybridization of renewable energy sources to create cleaner and more efficient solutions for vehicular transport. Various modular technologies exist, in which the traditional Internal Combustion Engine (ICE) driven by petrol is combined with an alternative energy source in the drive train. Hybrid designs, such as the Serial, Parallel, Combined, through the road, Two Mode, Micro and Mild, Full and Plug in Hybrids are currently being developed, tested and even commercialised. In this thesis, a prototype of the serial hybrid electric drive was designed to investigate the capability of combining a Hydrogen fuel cell and Lithium Ion Battery Power Pack to power a DC Motor using an embedded MSP430 Micro controller to control the Battery charging program. Basically, the system is a standalone battery charger combined with a DC motor, in which the DC motor is driven only by the Li-Ion Battery Pack while it is charged by the Hydrogen Fuel Cell. This hybrid electric drive system was designed at the Greenspace Research-Hydrogen Labs using the Heliocentris FC-50 PEM Fuel Cell to provide power to charge the Li-Ion Battery.

A complete analysis of the loading effect of the DC motor on the battery pack was done as observations were made on the charge and discharge states. An investigation into the variation of the DC motor speeds over a period of time (also known as a Drive Cycle) was executed. These Drive cycles were also generated to understand the impact of starts and stops as well as the impact of the charging program on the battery over a period of time, as a steady energy source is dissipated as it drives a load. Since this is a Prototypical Drive System, the basic properties of the drive train were measured and

analyzed, such as the Mechanical Power, Torque, Motor Speeds, Efficiency and Loading effect on the motor as drive cycles were emulated.

The specific objectives of this work are therefore to verify the efficacy of the embedded MSP430 microcontroller to charge the Li-Ion Battery pack when the DC motor is mobile and stationary, and understand the limits of the Li-Ion Battery pack as it drives the motor over a specified time period.

The next 4 sections of this thesis will cover the literature review of the current hybrid electric drive systems and more importantly the current serial drive systems available and prototypes in the market; this will be followed by methods and materials, which is the storyline of the research endeavour at the hydrogen labs at Greenspace Research involving the design, build and test phases of the different modules of this prototype; followed by Results and Discussion of the data acquired by the National Instruments Labview Signal Express Program and tachometer measurements of varying speeds over the different drive cycles as well as the analysis of this data; Finally, conclusions will be made and recommendations regarding future improvements on this prototype will be proposed.

2.0 Literature Review

2.1 The PEM Fuel Cell

The Polymer Electrolyte Membrane Fuel Cell or Proton Exchange Membrane Fuel Cell has a proton conducting membrane as the electrolyte. This electrolytic membrane is interposed between two platinum electrodes to enable faster electrochemical reactions at the electrodes. The electrode backing is Teflon coated and acts as a water proof and diffusion path for the Platinum catalyst to guarantee faster reaction rates. In Figure 2, the Anodic reactions release protons which diffuse through the polymer electrolytic membrane to the cathode where they react with Oxygen in an exothermic reaction to produce water. The electrons are conducted by a load generating an electric current.

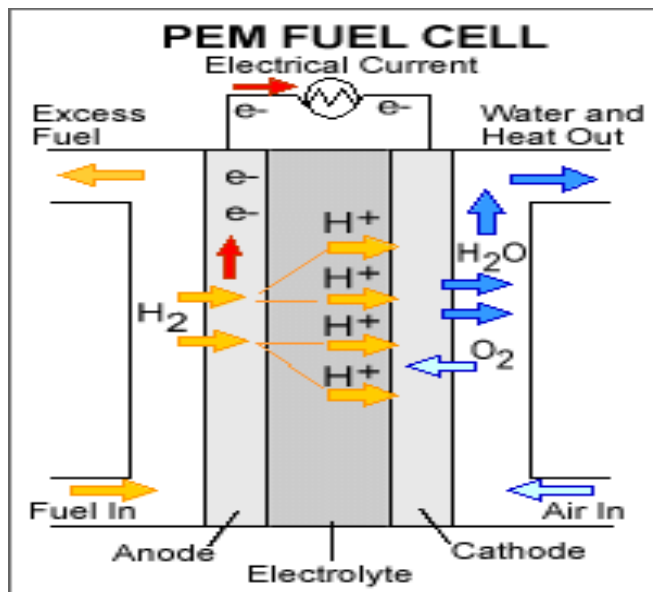
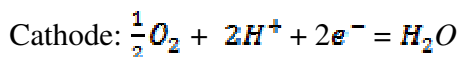
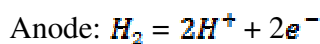


Figure 2 PEM Fuel Cell [3]

The Electrochemical reactions at both electrodes are shown below



The PEM Fuel Cell operates with Hydrogen as the primary fuel at relatively low temperatures giving them quicker start up times and reducing exposure to thermal stress, thereby increasing their lifetimes.

However, they are currently designed with Platinum catalysts which make them expensive and susceptible to catalytic poisoning from CO₂. Therefore, a clean Hydrogen gas supply must be guaranteed or a reformer module must be coupled with the supply to ensure that the CO₂ component is reduced.

Due to above mentioned ability to start up at low temperatures, PEM fuel cells have become a staple for transport applications. They also have a much more favourable Power to Weight Ratio enabling portability and increased range of operation. However, the drawback lies in the hydrogen storage as Hydrogen has a very low energy density and

a very low volumetric capacity (0.03Kg/L at 700bar) as well This implies that for a transport application, Hydrogen storage space will have a very high priority as compromises to the system design with respect to weight have to be made to enable the vehicle compete over the same distance as the petrol fuelled vehicles, due to the huge storage space required. [4]

2.1.1 Heliocentris Instructor-FC 50

The Heliocentris is a Power Supply Unit that has a PEM Fuel Cell. This power supply unit was deployed for this project. In figure 3, there are 6 components that make up the system. Five of which are on the main panel and the other is an external Data Acquisition Unit.

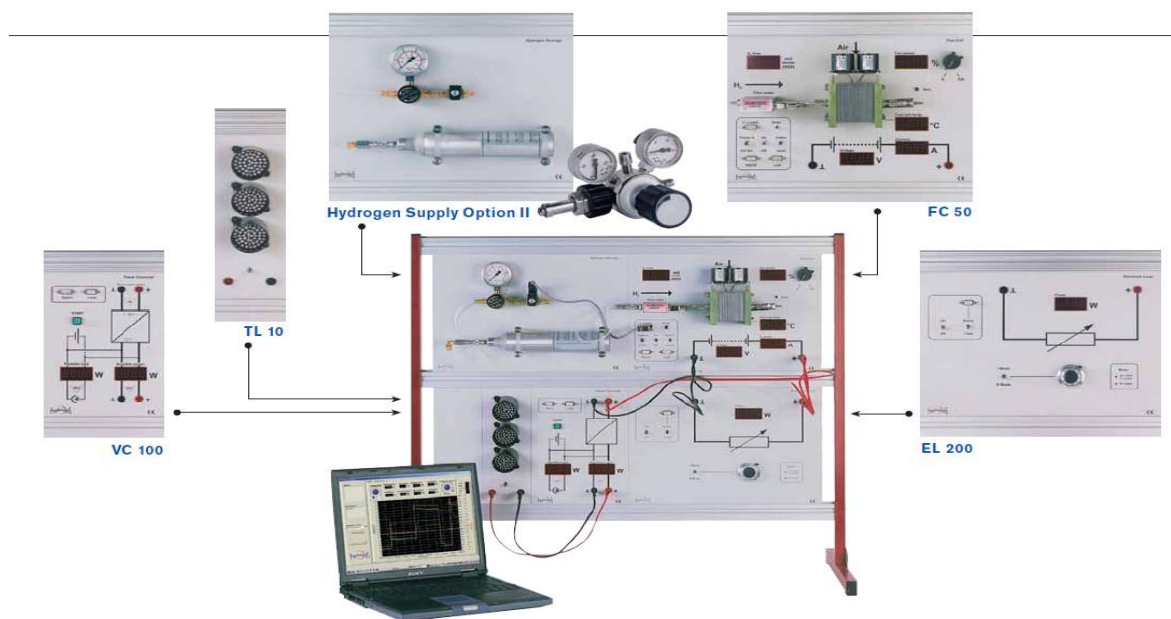


Figure 3 The Heliocentris Instructor [5]

The FC50 is the fuel cell stack, which is fuelled by gaseous Hydrogen from the Hydrogen supply cartridge and Oxygen from the fan intake. 5 LCD displays read out the cell temperature, output voltage, load current, hydrogen gas consumption rate and fan control. There are 10 cells in the stack that can produce a maximum power of 50W at 5VDC.

The EL200 on the main panel is the electronic load. It has a potentiometer that enables resistance values to be dialled in to create different characteristic curves.

The VC100 is a DC-DC voltage converter which provides a stable 12V supply voltage for applications such as Battery charging. It provides a stable 12V supply for the TL10 which is a traffic light and part of the experimental package for the Heliocentris Instructor.

Hydrogen Supply Option 2 is the metal hydride storage cartridge with quick coupler and single stage regulator. This provided the hydrogen necessary for the experiments at 10bar.

2.2 Lithium Ion Batteries

2.2.1 Origins

In the search for a lighter power pack for portable electronic equipment the Nickel Cadmium battery seemed to be the most suitable until the 1970s when the Lithium-Ion batteries made it to the scene and since then they have competed with the Ni-Cd batteries and are the most popular solution in the market.

Research for power solutions utilising Lithium metal (which is the lightest of all metals) began in 1912 under G.N. Lewis and continued until 1991, when SONY Corporation commercialised the first Li-Ion Battery [6].

2.2.2 Advantages

It has twice the energy density of the Ni-Cd batteries, with each cell having a high voltage of 3.6V. This allows for single cell battery designs as is available in cell phone batteries.

It does not suffer from the memory effect and has minimal self discharge compared to its competitors. It is also low maintenance as it does not need a periodic discharge.

2.2.3 Disadvantages

It is fragile and charge regimes must be controlled by internal protection circuits or microcontrollers to very accurate voltage ceilings. Temperature must be regulated as well during charge cycles. It tends to fail after 3 years, but there are certain models that have survived for 5 years. The metal Lithium is also a hazardous substance and transportation is controlled.

2.2.4 Charging the Li-Ion battery

A battery charger was designed for this project. This system which is based roughly on the Texas Instrument Li-Ion Battery Charger Solution implements the constant voltage charging process.

The constant voltage charging process is the fastest method utilised today in charging systems. It utilises a set voltage which is held constant while the state of charge of the battery will determine how much current will flow [ref]. Figure 4, shows the constant voltage process which was implemented with the MSP430F2132 microcontroller. This process was executed with the microcontroller sending a 50% duty cycle Pulse width modulated signal to the Li-Ion battery power pack during the above named process.

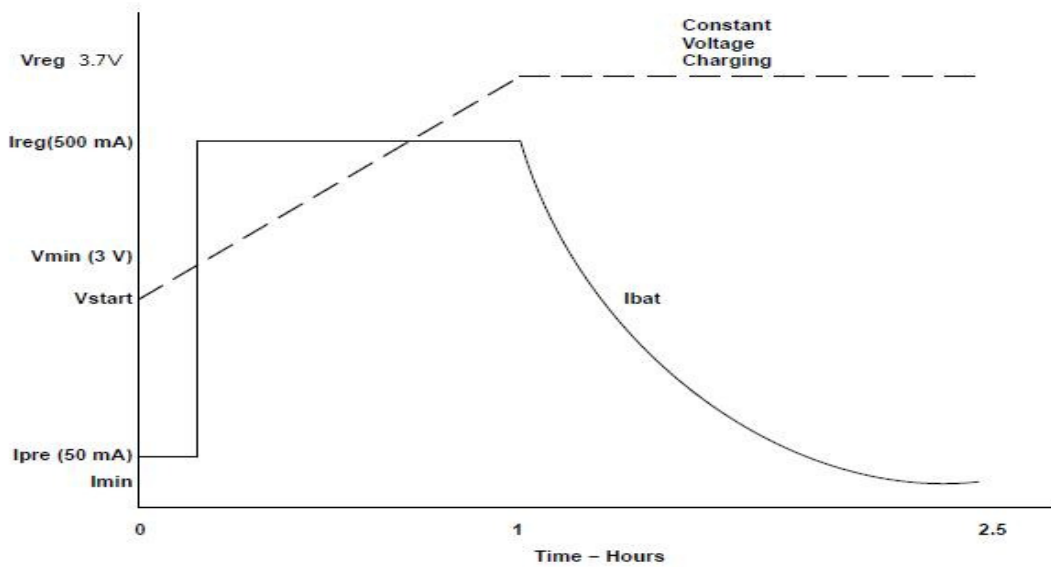


Figure 4 Constant Voltage Charge program for a 3.7V Lithium Ion Battery [8]

It is very important to note that as soon as the battery attains maximum voltage that the current begins to drop as the electrical energy becomes converted to thermal energy. This is where the charge controllers are useful such as the solution that was designed for this project using the MSP430F2132 microcontroller.

It is also important to note that a safe timing method can be employed, in which the battery charging process is timed and terminated when the time for a full recharge has expired.

2.2.5 Varta Li-Ion Battery Design

Due to the fact that it is the alkaline metal with the smallest molecular weight and it has a standard potential equilibrium of $-3.045V$, it is a very suitable material for negative electrodes which provide very high energy storage capacity. However, it can only be combined with organic electrolytes or molten salts as a result of its electro negativity and the electrodes in a Li-Ion battery dissolve during discharging and are reformed during the charge process. This leads to the formation of Lithium dendrites which can short circuit the electrochemical cell structure [8].

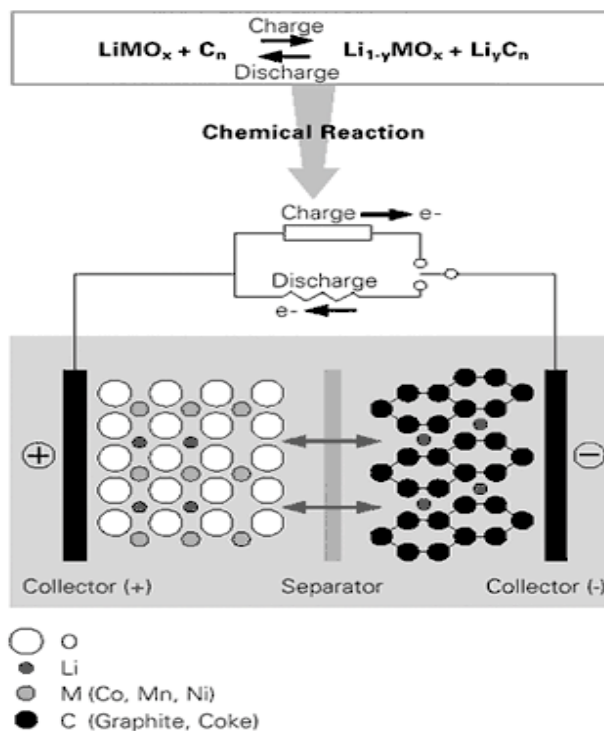
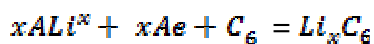


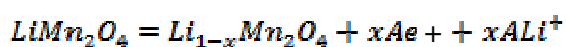
Figure 5a Basic Principle of the Lithium Ion Battery

In Figure 5a, a process known as Intercalation occurs during the discharging process (during which no real chemical combination of the chemical elements occurs in this process). The products of intercalation are compounds of Lithium combined with Graphite (basically Lithium ions interspersed beneath layers of graphite). During the discharge process the Li-Ions are released while electrons are absorbed or released at the same time as seen in this reaction:



In this reversible reaction, for every 6 carbon atoms, x Lithium ions are absorbed during the charge process. As the reaction proceeds in both directions the electrode potential remains constant.

At the positive electrode intercalation compounds of Manganese Oxides are formed as a result of the charge and discharge process represented by the reversible reaction below:



In the above equation adsorption means the active mass is discharged (going from right to left) while Lithium Ions are released during the charging process. If both electrodes are combined in a cell the Lithium ions migrate between both electrodes as shown in figure 5, this eliminates the problem of high solubility as the Li-Ions are highly soluble during the above reversible reactions. The Carbon and Manganese Oxides host grids at the electrodes remain unaltered, creating the ability to perform constant discharge and charge cycles without significant cell degradation.

The Lithium Ion battery has an Energy density of 120Wh/kg and can operate at room temperature [9].

Below is a diagram of the 3.7V Li-Ion battery that was deployed for this project. A very important subcomponent of this battery is its overcharge and over-discharge protection system (component 6 of figure 5b) which in subsequent chapters will manifest in data collected during discharge and charge cycles generated over the course of this project. This protection system protects the system to an overcharge voltage ceiling of 4.35V +/- 0.025V (with a delay/resume period of 0.4 to 2seconds at the 4.1V mark) and an over-discharge voltage floor of 2.3V +/- 0.08V (with a delay/resume period of 40/200milliseconds at the 2.8V +/- 0.1V mark). The watt hour rating of the Li-Ion battery shown in figure 5b is 7.3Wh.

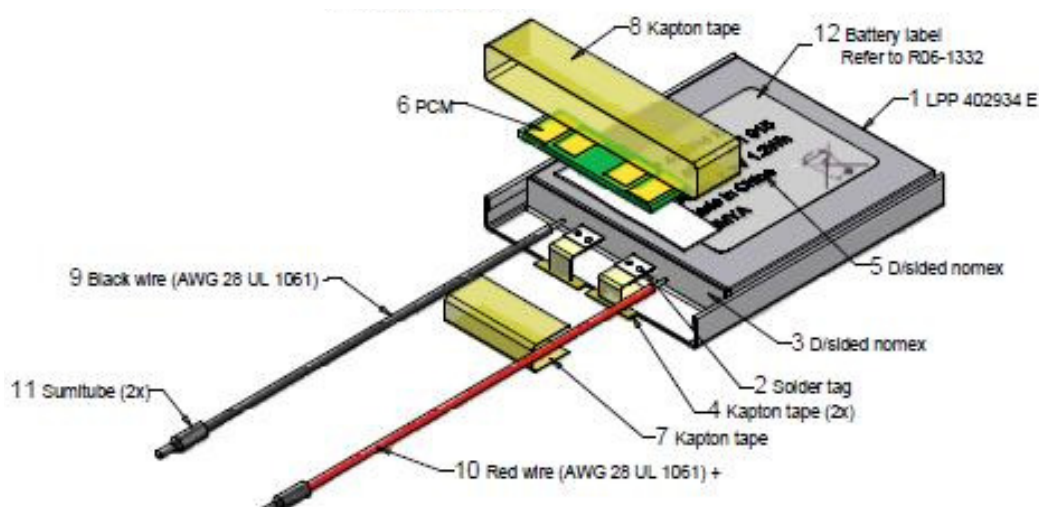


Figure 5b Varta Lithium ion battery with Protection Circuit Module [10]

2.3 Direct Current Motors

2.3.1 Description

They are devices that transform electrical energy to mechanical energy. They can possess a definite torque-speed characteristic or a highly variable one, meaning that they must be adapted to the load they are supposed to drive. In figure 6, when a DC motor is connected to a DC source a torque is produced as a result of the current flowing through the armature which is immersed in the magnetic field thereby causing the armature to rotate. A counter-electromotive force is developed in the armature as it cuts the magnetic field. This CEMF is expressed in the following equation

$$E_o = Z n \Theta / 60$$

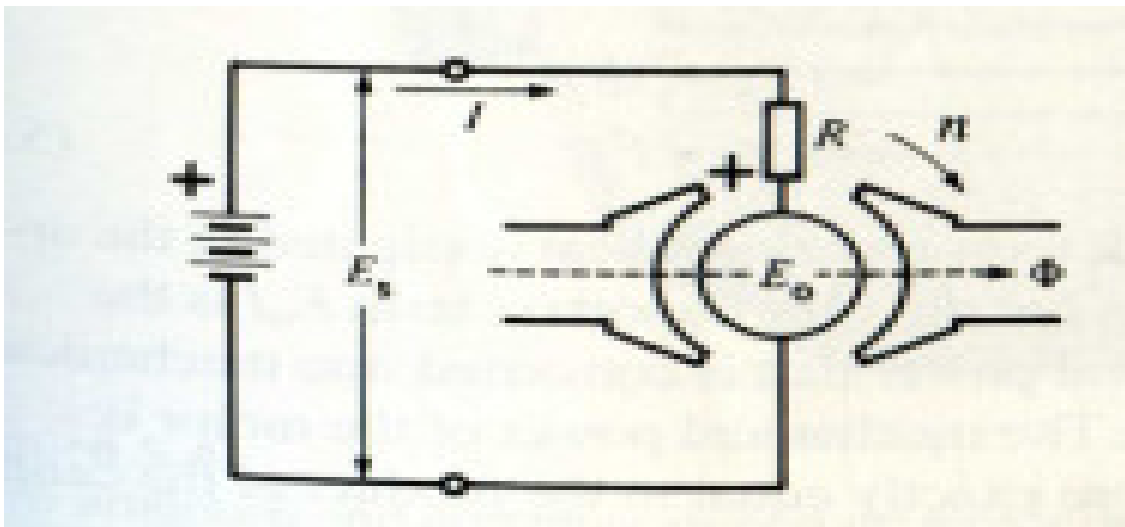


Figure 6 CEMF in a DC motor [11]

Where Z is a constant that depends on the number of turns of the armature and the type of winding; n is the speed of rotation of the motor and Θ is the flux per pole. The net voltage

acting on the armature in Figure 6 is $(E_s - E_0)$. The armature current is limited by the resistance in the armature. Therefore;

$$I = (E_s - E_0)/R \dots \text{when the armature is mobile.}$$

And

$$I = (E_s)/R \dots \text{when it is stationary, because the CEMF is zero as no voltage is induced.}$$

As soon as the armature starts rotating, E_0 approaches E_s leading to a decrease in the armature current, this leads to a speed decrease. However, the motor accelerates to a definite maximum speed. At no load E_0 is slightly less than E_s . It is important to note that they cannot be equal as this will cause the motor to halt. As the speed decreases, the net voltage increases with the current and the motor speed will cease to fall when the torque developed by the armature current is equal to the load torque.

2.3.2 Mechanical Power

This property of a DC Motor depends on two other important properties, the rotational speed and torque of the DC motor. Where they are related by the equation:

$$P = nT/9.55$$

The mechanical power is derived from the Power Supplied to the armature, which is the product of the supply voltage multiplied by the armature current as expressed in the equation below:

$$P_a = E_s I$$

Applying Kirchhoff's Voltage Law to Figure 6 and expanding the relationship;

$$P_a = (E_0 I + IR^2)$$

Thus, the Mechanical Power is $P = E_a I$ is the electrical power converted to mechanical power. The second term represents heat losses from wind resistance and hysteresis in the armature.

2.3.3 Mechanical Torque

The Mechanical Torque is inversely proportional to the speed of the rotating motor and directly proportional to the mechanical power. This means it is also directly proportional to the product of the flux and number of conductors on the armature. See the expression below:

$$T = Z \Theta / (6.28) = 9.55 P / n$$

This property originates as a result of the CEMF on the armature that enables it to rotate.

2.3.4 Speed of Rotation

The speed of rotation is directly proportional to the supply voltage as will be demonstrated in subsequent chapters. There is very minimal difference in the IR drop as a result of the armature resistance when the motor moves from no load to full load. This means E_0 , the Armature voltage can be replaced with E_a in this equation:

$$E_0 = Zn\Theta/60$$

Therefore, $E_a = Zn\Theta/60$ and the speed of the motor is:

$$n = 60 E_a / Z\Theta$$

2.3.5 Mechanical Efficiency

All known energy transfers involve losses. For machines that have rotating parts these losses are known as mechanical losses. They are due to windage, brush friction and can

be minimised by optimising the design of the contact surfaces and utilizing better cooling fans and air flow control systems in the machine housing.

The Efficiency of a DC motor is the ratio of the useful output power to the input power as expressed in the equation below:

$$\text{Efficiency, } \eta = P_o / P_i$$

[11]

2.4 Electric Drive Technologies

Four major motor drives are currently in service today. They are the Brushed DC, Permanent Magnet (PM) Brushless DC (BLDC), Induction (IM) and Switched Reluctance (SRM) Motor Drives.

Brushed DC motor drives have the ability to achieve high torque at low speed and are well suited for traction equipment. However they are rugged and bulky with low efficiency and are expensive to maintain. The presence of brushes and commutators reduces the motor speed and adds to their overall weight.

IM drives are simple, less expensive and operate in hostile environments. They do not have brushes and so their speeds are higher than the Brushed DC motor drive. They have expensive controllers and a limit to the Torque known as Breakdown Torque (i.e. the torque at critical speed, at which any attempt to operate the motor at maximum current will cause a stall) that limits extended constant operation.

PM BLDC motor drives have higher efficiencies and power densities. This is due to the fact that the presence of the permanent magnet eliminates the need for electrical energy to produce magnetic poles. Their speeds and efficiencies rival the competition by 3-4 times.

They are expensive due to the cost of magnetic material and the field strength tends to weaken over time due to the production of a stator field component.

SRM are new and gaining popularity because of their simplicity in terms of design, operation and control. They also have outstanding torque-speed characteristics and unlike the IM drives can operate over extended periods of constant power. Due to its low rotor inertia and simple design, it has a higher fault tolerance. It also has good IR reduction measures as there are no magnetic sources to induce hysteresis. However, they can be noisy and suffer from torque ripple (Selection of Electric Motor Drives for Electric Vehicles) [12].

2.4.1 Electric Drive Hybridisation

The term Hybrid Vehicle as defined by the United Nations is a vehicle with 2 different energy converters and 2 different energy storage systems for the purpose of propulsion. There are three basic architectures of vehicle drive train hybridisation: Series Hybrid, Parallel Hybrid and Series-Parallel Drive Trains or Combined Drive Train.

2.4.2 Serial Hybrid Drive

In the Series or Serial hybrid drive, the combustion engine directly drives an electric generator instead of the wheels. The electric generator then charges the battery pack which drives an electric motor that propels the vehicle. This is the case in the prototype designed for this project. The only difference is that the combustion engine is replaced with a hydrogen PEM fuel cell. There is no mechanical link between the PEM fuel cell and the motor allowing maximization of the energy density of the fuel cell and efficient dispatch of energy for start and stop situations. In a real motor vehicle, the serial hybrid implementation with internal combustion engine (ICE) must have the energy pass from the generator to the motor. During extended drives, IR losses accumulate as a result of this electrical transmission making it less efficient than conventional transmission. Figure 7 shows the series hybridisation of the two power trains (i.e. Battery and ICE). The GM Volt which will be available in 2020 is an example of the Serial Hybrid.

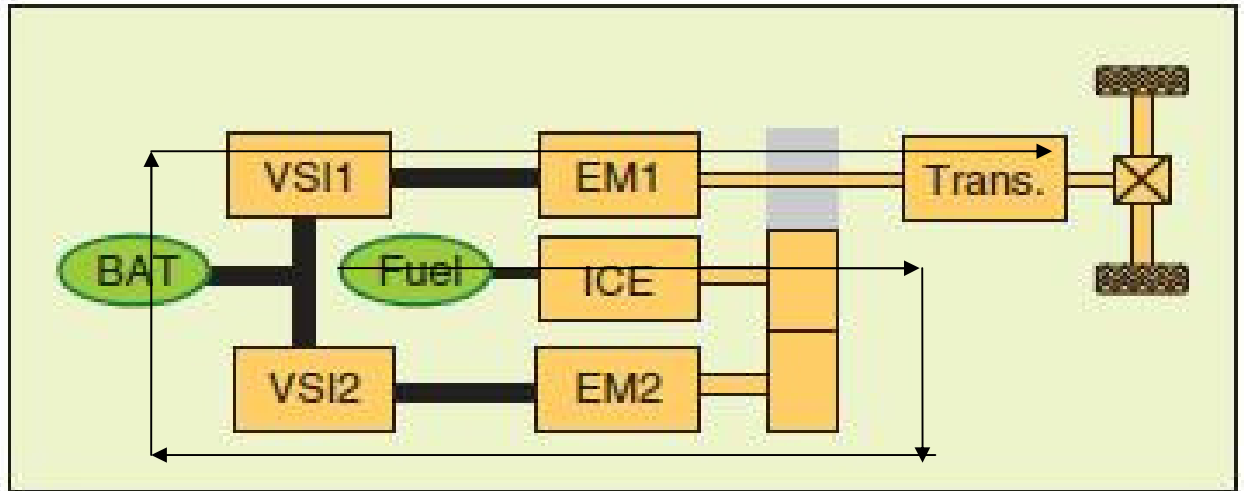


Figure 7 Serial Hybridization of Battery and ICE Power trains [13]

In figure 7, VSI 1 and 2 are voltage source inverters which invert the DC voltage signal from the battery to provide AC Voltage to the EM 1 and 2 which are Electric Motors. Please, observe the serial arrangement of the power trains by following the black arrow.

2.4.3 Parallel Hybrid Drives

The Parallel Hybridization system involves the connection of both powertrains alongside each other to the mechanical transmission system. Today, they are designed by combining the large generator with the motor to replace the starter motor and alternator. A larger battery than the conventional 12V battery is used to store energy so that other accessories can be powered more efficiently regardless of the speed of the motor. In Figure 8, the power trains are coupled by a differential gear which allows the input speed to be controlled.

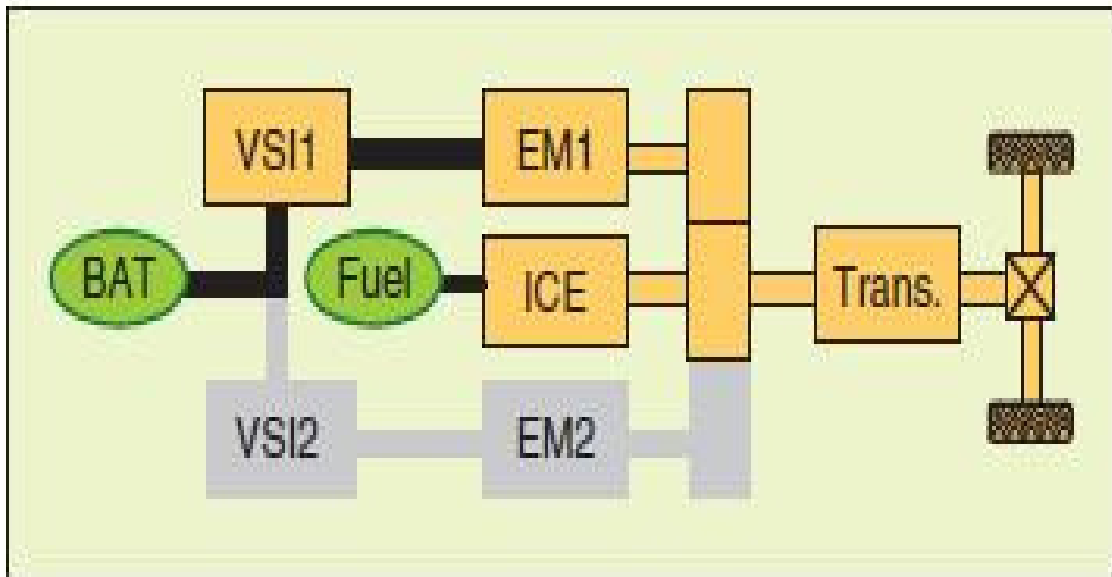


Figure 8 Parallel Hybridization of the ICE and battery powertrains [13]

This coupling allows for the ability to choose the dominant part of the drive train, be it the ICE or the battery or both. The Toyota Prius is a good example of the parallel hybrid.

2.4.4 Combined Hybrid Drives

Combined or Series-Parallel Hybridization involves both features of the serial and parallel drive trains. They utilize power split devices that control the path of power from the two powertrains. This allows for decoupling of the ICE power or the primary power from the driver controls. Typically, the combined hybrid will have a smaller more efficient engine than the ICE that will allow it to generate maximum torque at low rpm during stall conditions and acceleration from standstill. Figure 9 is a combined Hybrid which possesses a planetary gear unit with Ring (R) and Sun (S) gears and a Carrier (C) – see figure 10. It is observed that the system is much more complicated and expensive as the different drive trains can be coupled and decoupled by the planetary gear system via the DC bus. Observe that the electric motor shares a common shaft with the transmission shaft and all three machines are connected together via the carrier in figure 9.

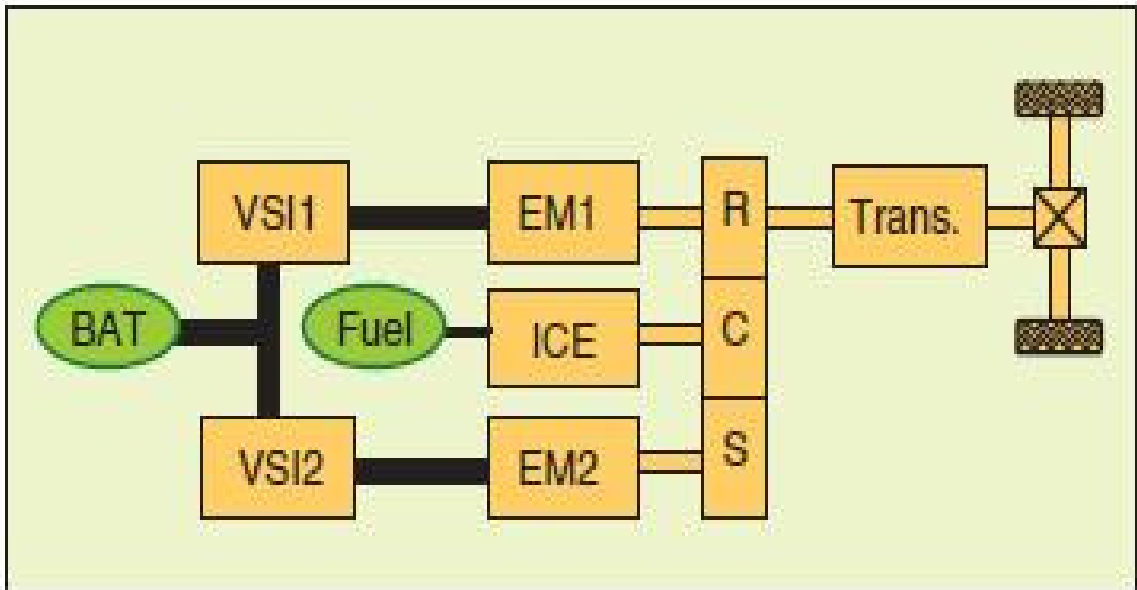


Figure 9 Series-parallel or combined hybridization

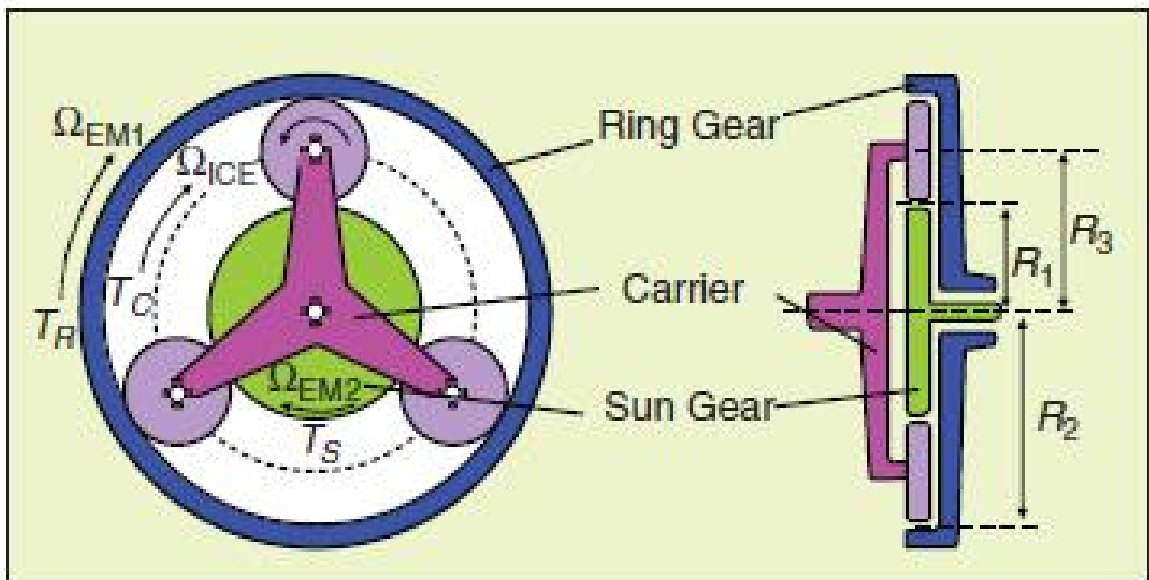


Figure 10 Planetary Gear System: T and Omega represent Torques and Correspondent speeds in the electric motors and the different components of the planetary gear unit.

Other Hybridization technologies exist, such as through the road hybrids which have independent powertrains that operate on separate axles. The ICE and Electric motor combine power when more power is needed and then the ICE powertrain is disconnected to allow the electric powertrain kick in. Regenerative Braking allows for battery charging and the system uses the energy more efficiently in the 4 wheel drive configuration because energy from the ICE is activated only during heavy traction. Otherwise, the electric motors in the electric powertrain provide traction.

There is also the two mode technology which Daimler is currently deploying. GM and BMW use an electric continuously variable transmission, allowing their vehicles to operate at high efficiencies and economise fuel using a four fixed ratios gear system. It has improved torque speed characteristics as a result of the implementation of the electric continuously variable transmission.

Full Hybrids can either run on the ICE alone or the battery system or both such as the Toyota Prius. When the battery can be connected to the national grid it is called a Plug in Hybrid Electric Vehicle.

There are also varying degrees of hybridization, which range from micro to mild. The difference lies in the presence of large starter motors in both conventional vehicles and the ability to cleanly engage and disengage the engine during starts, cruise and stop conditions. [14]

2.5 MSP430F2132 Mixed Signal Microcontroller

2.5.1 Description

It is an ultra low power (i.e. Active mode-250uA, 2.2V; Standby mode-0.7uA; Off-mode-0.1uA) microcontroller for portable applications. It has 2 built in 16bit timers with capture compare registers to register events, a 10 bit Analogue to Digital Converter (ADC) with integrated reference and data transfer controller that can operate in 5 low power modes. It has a unique 16bit RISC (i.e. the instruction set for the chip architecture

allows for word and byte data assignments to the sixteen 16-bit registers, there are 51 of these instructions that operate at 62.5ns cycle time) and a Basic Clock Module that can be configured for frequencies up to 16MHz. There are 28 pins on the micro controller as shown in figure 11. These input and output (I/O) pins provide digital and analogue access to the internal devices on the chip and to peripheral devices like the tuning fork or resonator for high frequency applications.[14]

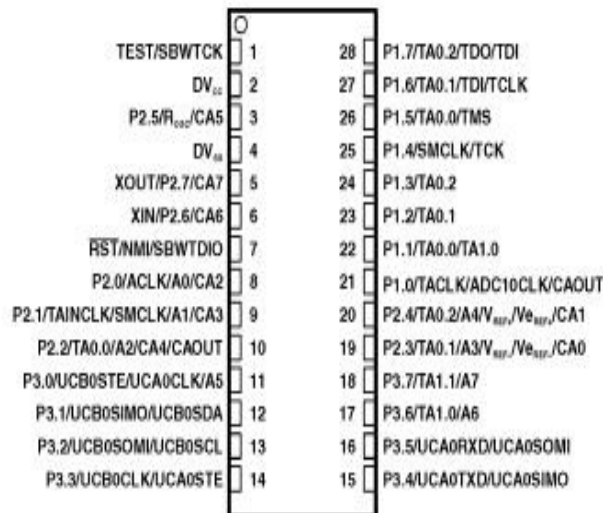


Figure 11 I/O Pins

The system architecture of the MSP430F2132 has 27 instructions and 7 addressing modes that allow for programming in assembly and C. Programming for this project was done in assembly. The architecture is orthogonal allowing for the same instructions to be used in all the addressing modes. The architecture is shown in figure 12.

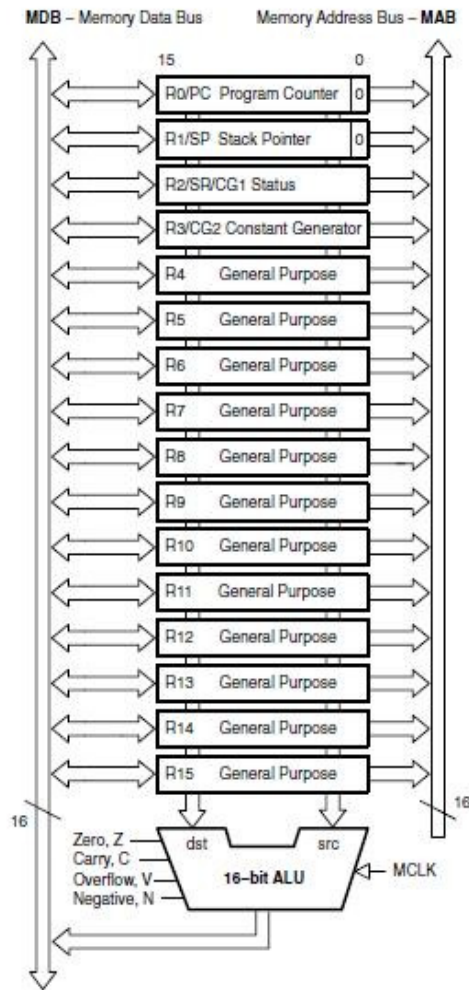


Figure 12 MSP430 CPU Architecture

In Figure 12, the first register is the program counter which points to the next instruction to be executed in the source code and is incremented by 2, 4 or 6 depending on the number of bytes for that instruction. The Stack pointer is used to store return address of subroutine calls and interrupts during the execution of source code to enable a logical and correct return to the program execution when subroutines are called. The status register contains status bits that are set or cleared after carries, zero sum, overflow or negative operations are executed. It also has the General Enable bit for maskable interrupts, the CPU off bit, the Oscillator off bit and the system clock generator bits to turn of the clocking and oscillator systems. The constant generators generate 6 commonly used

constants without requiring additional code. The last set of registers are general purpose registers used for data transfer, index values and pointers. They can be accessed by the 27 core instructions in either byte (8 bit) or word (16bit) format.

2.5.2 Operating Modes

There is one active mode of operation for the MSP430F2132 and 5 Low Power Modes (LPM) for controlling the events in the source code. This is so that power is efficiently consumed and data movement is controlled effectively and in a timely manner. The battery charger in this project was programmed to operate at low power mode 0, during which the CPU is disabled and the Auxiliary clock (ACLK) and Sub-Main Clock (SMCLK) remain active while the Main Clock (MCLK) is disabled. All the Low Power Modes have the CPU disabled; However, LPM1 has the ACLK and SMCLK active while the MCLK is disabled. The Digitally Controlled Oscillator (DCO) remains active if it is used in the active mode, else it is disabled. LPM2 has CPU, MCLK, SMCLK disabled while the DCO and ACLK stay active. LPM3 has DCO, CPU, SMCLK and MCLK disabled while the ACLK remains active. In LPM4, all the clocks and oscillators are disabled. Below is a diagram showing all the operating modes available for the Basic clock.

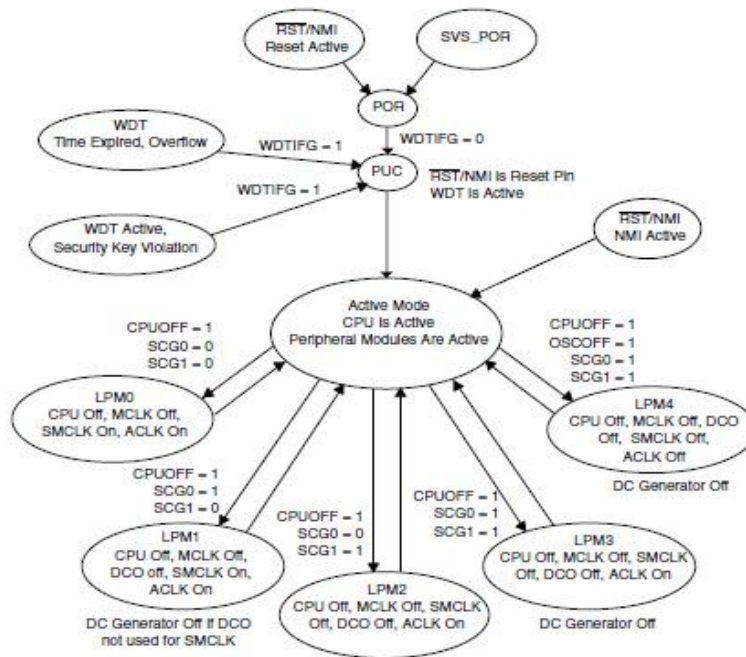


Figure 13 Operating Modes of the MSP430F2132

2.5.3 Digital Input and Output

The MSP430F2132 has eight digital I/O ports that can read and written to. They appear as pins on the PCB (Printed Circuit Board) can also be configured for input, output, direction, Pull-up/Pull down Resistor Enable, Function Selection, Interrupt flag and Interrupt enable capability. Only Pins 1 and 2 have Interrupt Capabilities, they share the other capabilities with the other pins.

2.5.4 Timers

Timer A (TA) was used in this project for the timed charge routine. In figure 14, the 16bit counter (TAR) has 3 capture/compare (TACCR0, 1, 2) registers and generates pulse width modulated (PWM) signals which can be output to the digital output pins. It can also provide interval timing as well to enable the execution of timed events. It also has interrupt capabilities as well, enabling an interrupt when there is an overflow condition in any of the capture compare registers.

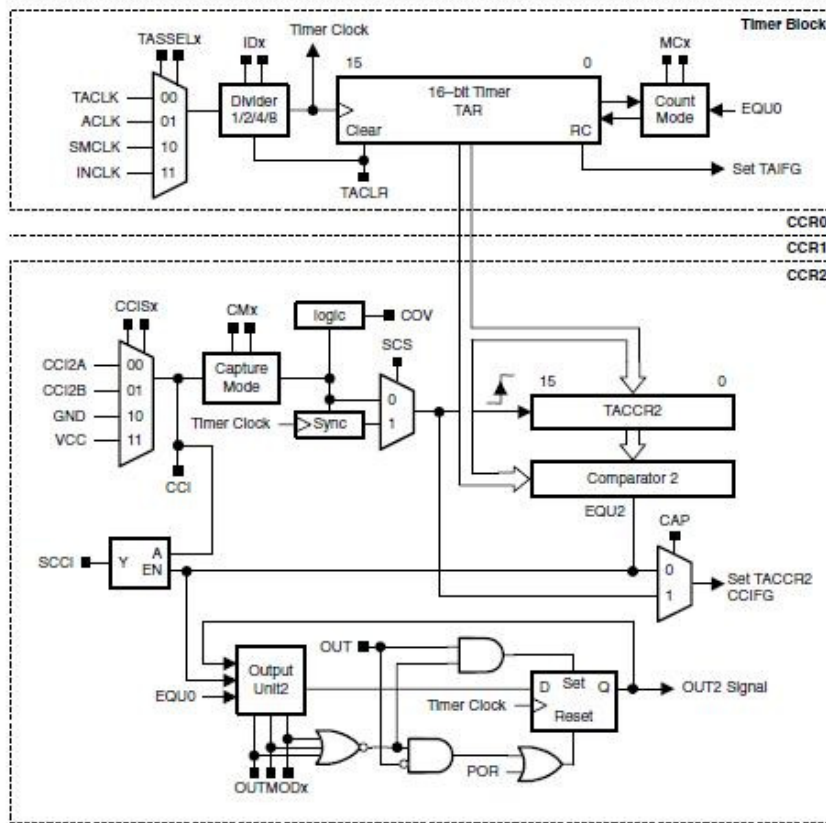


Figure 14 Timer A

2.5.5 Analogue to Digital Converter (ADC)

The 10bit ADC supports fast A/D conversions. The 10bit core converts analogue input to 10bit digital representation which is stored in the ADC10MEM register. This is done by using two programmable/selectable voltage levels (VR+ and VR-) to define the upper and lower limits of the converted value which in this project is the voltage signal of the Lithium Ion-Battery pack. The process is controlled by the ADC10CTL registers that possess control bits for configuring the A/D conversion. This process must be clocked effectively and the ADC10CLK provides the sampling period which is sourced from the ADC10OSC, MCLK, SMCLK or ACLK. Figure 15, shows the 10 Bit ADC. It also has sample select control ADC10SSEL, Reference generator, Data Transfer Control (DTC) so as to guarantee automatic data conversion without CPU intervention.

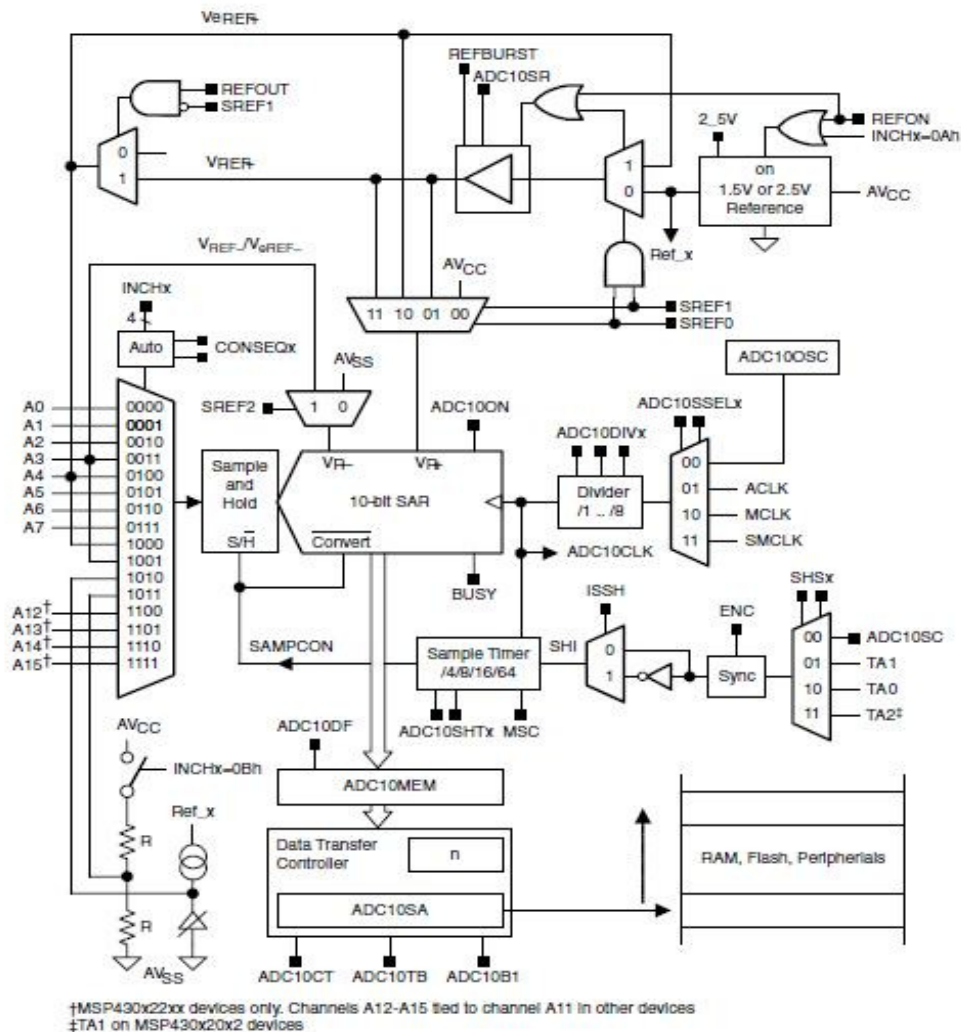


Figure 15 10bit ADC [15]

3.0 Methods and Materials

Inspiration for this project was drawn from the Texas Instrument Li-Ion battery charger solution and the project was nicknamed volTRONE (VOLTRON is a Japanese cartoon series I watched as a child. Voltron is formed by 5 Lion robots. Once the Lions are integrated, they form a gigantic robot that defends the universe from its enemies).

this circuit) of the Inductor and capacitor on the back end of the buck inverter, the voltage of the capacitor is held constant and is equal to the mean input voltage to the buck converter. Only 1 channel is monitored by the microcontroller program, A0. This channel is directly connected to the positive terminal of the battery and the ADC interrupt service routine was written to detect voltages as low as 0.3V and as high as 1.45V. At the 1.45V level the battery has charged ending the interrupt routine and starting a terminate charge subroutine. Thereby, stopping all the timers and the ADC sampling process. This will be shown in subsequent subsections of this chapter.

The hybrid serial drive system consists of 5 main modules. They are: the Data Acquisition module, Microcontroller Module, Voltage Regulator and Power Module, DC Induction Motor Electric Drive and the PEM Hydrogen Fuel Cell System as shown in the block diagram in figure 17b.

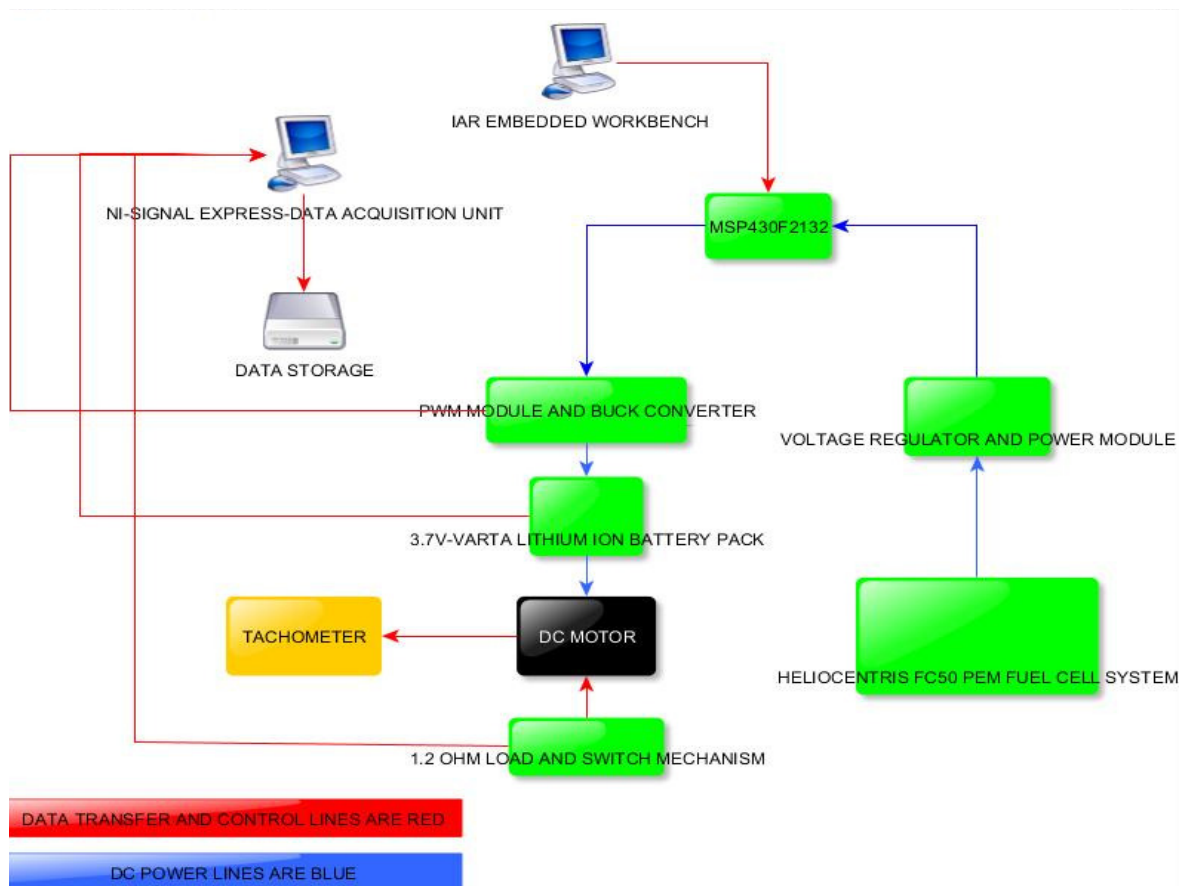


Figure 17b Block Diagram of Hybrid Electrical Serial Drive System (aka volTRONe)

The Microcontroller Module is composed of an Alienware Laptop PC equipped with a dual core AMD Athlon computer which runs the IAR embedded workbench Integrated Development Environment on which the Microcontroller source code was developed, tested and deployed. This module also includes the MSP430F2132 Mixed signal Microcontroller which provides the Pulse Width Modulated Pulsed Voltage signal to the Lithium Ion Battery pack and acquires its voltage signal for A/D conversion. It is in this module that the Sourcecode is downloaded to the MSP430F2132 and executed.

The Data Acquisition Module (see figure 18) is made up of basically my laptop which is an acer Extensa 5220 with an intel Celeron processor and a Buffalo HDD with 300GB capacity. The National Instruments Labview Program known as Signal Express runs the Data Acquisition Task. It collects data from 4 streams via the NI USB 6088 DAQ, which has 8 (12bit) inputs that can sample (digital and analogue) data streams at 10Kilo Samples per second: The Voltage signal from the Li-Ion battery, the current signal from the Li-Ion battery, the Voltage signal from the fuel cell and the digital pulses generated by the pulse width modulation module. There is also a tachometer attached to the system to measure the motor's speed.

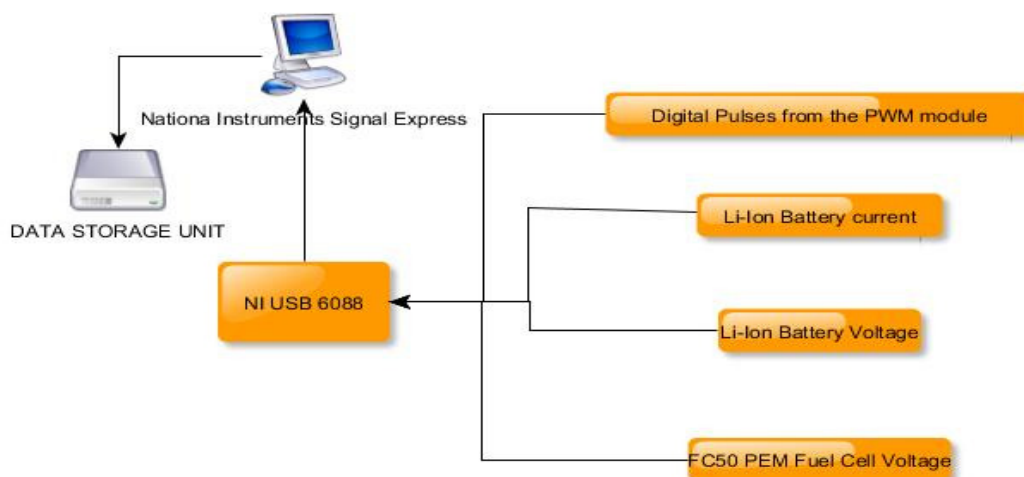


Figure 18 Data Acquisition Module

In figure 19, a panel of the data acquired during a charge program is played back showing the four different channels that were sampled, including timestamps and signal behaviour over the period of the program. Please, observe the 50% duty cycle signal at the bottom part of the panel. This is evidence of the microcontrollers ability to pulse Port 1.1 and create the PWM input of power from the FC50 PEM fuel cell. The signal has some noise, which is acceptable because the circuit was built on a breadboard and other devices sharing the board such as the electronic control unit from the Heliocentris and the computers could have generated some noise.

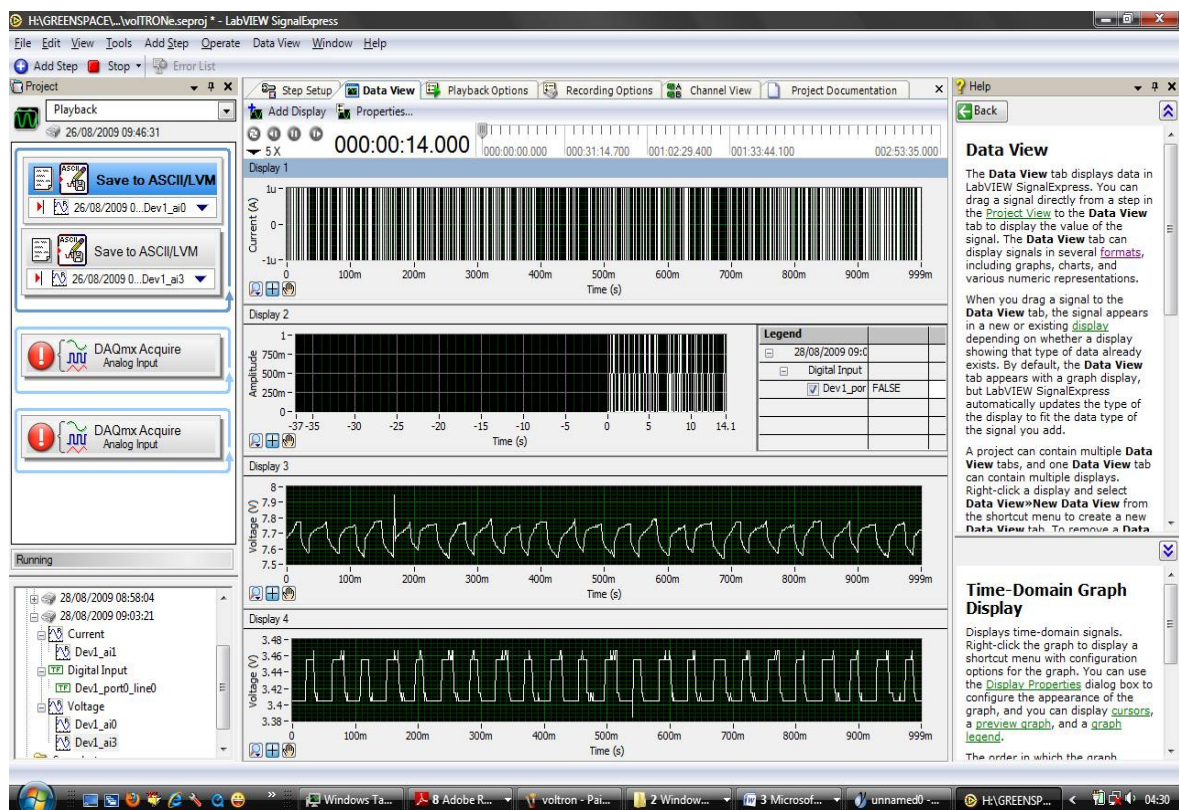


Figure 19 NI-Signal Express Data Playback of charge program.

The voltage regulator module and power module was implemented with the 1.5A Adjustable Output Positive Voltage regulator, known as the LM317 or NCV317. It can provide voltage outputs up to 37V. It has 3 terminals and two 1Kohm resistors were used to adjust the voltage supply (VCC) to the Microcontroller to provide the precise voltage

output. Figure 20, shows the configuration that was used in the serial hybrid system designed for this project.

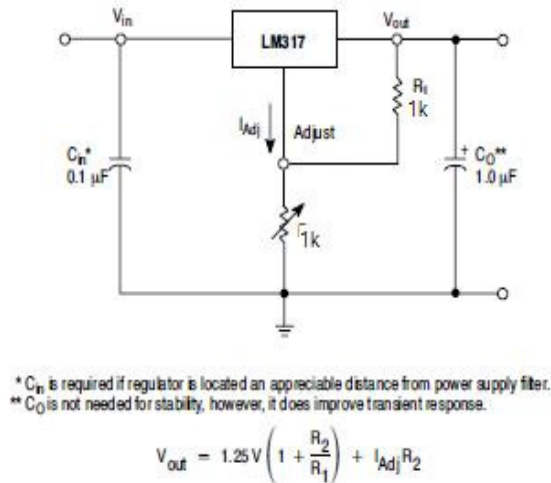


Figure 20 Voltage Regulation Module.

The DC Electric Drive Module is composed of the Li-Ion battery, the DC motor and the switch gear for loading the motor to simulate different drive cycles. From figure 17b, the system is loaded with a 1.2ohm-300W resistor to draw more current from the battery to emulate different inclines if the motor was deployed to turn the wheels of a tire.

3.1.1 MSP430 Microcontroller Battery Charger Programme Design Environment

One major endeavour during this project was to design a battery charger controlled by the MSP430F2132. This was achieved by writing a program in the IAR systems IDE to efficiently deliver power from the FC50 to the Varta Li-ion batteries using pulse width modulation from the MSP430 and the constant voltage charging method. Below is a block diagram of this system.



Figure 20a Battery Charger Block diagram

The microcontroller programme was designed using the IAR systems Embedded Workbench IDE (Integrated Development Environment). This IDE integrates the following systems: a compiler, assembler, linker, builder, word editor, MS DOS utility and a high level language debugger all managed by the efficient project manager. It is a very versatile IDE and can be used for developing projects used by many of the processors in the today's market. This workbench can be deployed as a Flash Emulation tool debugger or a Simulator. The assembler was used extensively for this project to write the source code because it uses the same mnemonics and syntax as the TI MSP430 assembler allowing portability. This assembler has a C-Pre-processor, 255 significant characters in symbol names, up to 65536 relocatable segments per module and support for complex expressions with external references. The Linker links Assembler source code to the Compiler to produce machine code for the MSP430 which is the object file that is downloaded to the microcontroller. After the program has been written, it can be built and then debugged [ref].

3.1.1a Charge control Algorithm

Figure 20a is a representation of the charge algorithm. Basically, the program starts with the initialisation of the Stack pointer to CSTACK allowing access to memory locations 0x0002 to 0xFFFFD. Then the 10bit ADC is enabled to do a repeated multichannel sample of channel A0 and do a sample and hold of the analogue voltage values from channel A0. The Basic Clock is then set up using the low frequency oscillator while the Master Clock is set up to time the digitally controlled oscillator.

The ADC core is then checked for activity, with an LED at Port 1.1 coming on if data is streaming through A0. The RAM location for the storage of the voltage data values is initialised to 0x200. The Basic timer which will be used to do a safe time charge by counting up to 30 minutes, which is the time for a stationary charge with the DC motor disconnected. The BCSETUP subroutine sets up Timer-A to count up and initialise the registers that will store the minute and second values.

Once this is all done the clock subroutine is executed in LPM0 and the count up (as opposed to count down) is executed. Every time the loop is exited the voltage is checked to see if the battery is charged. The CPU is then turned off to conserve power and then The LED on Port 1.1 is pulsed at a 50% duty cycle to create the PWM effect necessary to effectively dispatch power from the FC50 PEM fuel cell. The frequency of the signal is designed for 1.5 kHz if the crystal oscillator is connected to the MSP430F2132.

Also included are snap shots of the Source code to match with the algorithm, See figure 20c.

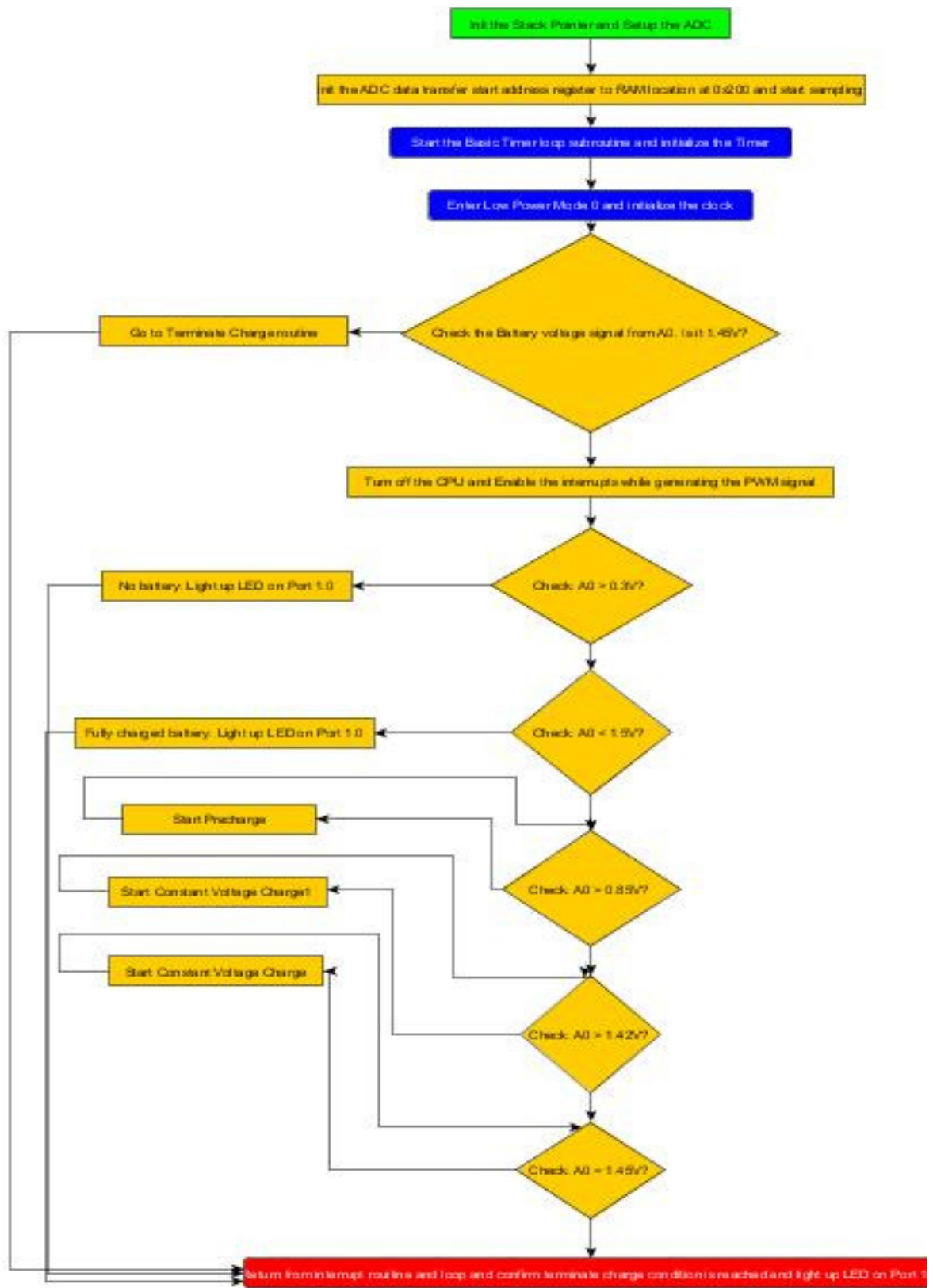


Figure 20b Flowchart showing the charge algorithm

```

;*****
; MSP-FET430F2132 - ADC10, Repeated Sequence of Conversions
;
; Description: This program will show how to perform a repeated sequence of
; conversions using the "repeat sequence-of-channels" mode.
;
; A repeated sequence of conversions is performed on Channel A0 using ADC10.
; Each conversion result is stored in ADC10MEM; After each sequence,
; the conversion results are moved to ram locations.
; The conversion results for channel A0 are
; moved to ram addresses 0x200 - 0x20E. The program is Tested by
; applying voltages to channels A0.
;
; Timer A is used to execute a safetiming charge and a pulse width modulated
; signal is generated on P1.1 to efficiently utilise power from the fuel cell
;
; JOHN EGBUTA
; ESRU, UNI. STRATHCLYDE
; JULY, 2009
;*****
#include "msp430x21x2.h" // Standard Equations
#define SEC R13
#define MIN R14
;-----
; RSEG CSTACK ; Define stack segment
;-----
; RSEG CODE ; Assemble to Flash memory
;-----
RESET mov.w #SFE(CSTACK),SP ; Initialize stackpointer
StopWDT mov.w #WDTPW+WDTHOLD,&WDTC1L ; Stop WDT
SetupADC10 mov.w #INCH_2+CONSEQ_2,&ADC10CTL1 ; A1,A0, repeat multi channel
mov.w #ADC10SHT_3+MSC+ADC10ON+ADC10IE,&ADC10CTL0 ;
bis.b #07h,&ADC10AEO ; P2.0,1,2 ADC option select
mov.b #060h,&ADC10DTC1 ; 96 conversions
SetupP1 bis.b #002h,&P1DIR ; P1.1 output
SetupBC bis.b #LFXT1S_2,&BCSCTL3 ; LFXT1 = VLO
SetupOsc bic.b #OFIFG,&IFG1 ; Clear OSC fault flag
bis.w #SCG1+SCG0,SR ; Stop DCO
;-----
bis.b #07h,&ADC10AEO ; P2.0,1,2 ADC option select
mov.b #060h,&ADC10DTC1 ; 96 conversions
SetupP1 bis.b #002h,&P1DIR ; P1.1 output
SetupBC bis.b #LFXT1S_2,&BCSCTL3 ; LFXT1 = VLO
SetupOsc bic.b #OFIFG,&IFG1 ; Clear OSC fault flag
bis.w #SCG1+SCG0,SR ; Stop DCO
bis.b #SELM_3+DIVM_3,&BCSCTL2 ; MCLK = DCO
SetupP1_2 mov.b #004h,&P1DIR ; All P1.x outputs
clr.b &P1OUT ; All P1.x reset
Mainloop bis.b #002h,&P1DIR
busy_test bis.b #002h,&P1OUT ; P1.1 = 1
bit #BUSY,&ADC10CTL1 ; ADC10 core inactive?
jnz busy_test ;
mov.w #0200h,&ADC10SA ; Data buffer start
bis.w #ENC+ADC10SC,&ADC10CTL0 ; Start sampling
loop bis.b #004h,&P1OUT ; Set P1.2
BASIC_TIMER CALL BCSETUP
bis #LPM0, SR
CALL CLOCK
cmp #03B6h,&ADC10MEM ; A0=1.45V
JEQ TERMINATE_CHARGE
bis.w #CPUOFF+GIE,SR ; CPU off, Enable interrupts
bic.b #002h,&P1OUT ; P1.1 = 0
Delay1 mov.w #0128,R15 ; Delay to R15
L1 dec.w R15 ;
jnz L1 ;
bic.b #004h,&P1OUT ; Reset P1.2
Delay2 mov.w #0256,R15 ; Delay to R15
L2 dec.w R15 ;
jnz L2 ;
cmp #001,R15
jeq prima ; Again
jmp loop ; Again
prima jmp Mainloop ; Again
CLOCK SETC
DADC.B SEC

```

```

        CMP.B    #060h, SEC
        JLO     CLOCKEND
        CLR.B    SEC
        DADC.B  MIN
        CMP.B    #030h, MIN
        JLO     CLOCKEND
        CLR.B    MIN
CLOCKEND
        RET

BCSETUP    bis.b    #008h, &P1DIR           ; P1.3 output
           bis.b    #008h, &P1SEL         ; P1.3 TA1 options

           MOV #TASSEL0+TACL, &TACTL
           BIS #CCIE, &TACCTL2 ; Enable CCR0 interrupt.
           MOV #07FFFh, &TACCR2 ; load CCR2 with 32,767.
           BIS #MC0, &TACTL ; start TA in "up to CCR2" mode
ClearRTC   MOV.B    #00h, SEC ; Clear SEC
           MOV.B    #00h, MIN ; Clear MIN

           EINT ; Enable interrupts
           RET ; Done with setup.

;-----
ADC10_ISR;
;-----

           bic.w    #ENC, &ADC10CTL0      ; ADC10 disabled
           bis.w    #CCIE, &TACCTL0      ; Compare-mode interrupt
           bic.w    #LPM0, 0(SE)         ; Exit LPM0 on reti
Check_0_3V  cmp.w    #00C5h, &ADC10MEM    ; ADC10MEM = A0 > 0.3V?
           JHS     Check1_5V
           jmp     NO_BATT_OR_FULLCHARGE

Check1_5V   cmp.w    #03D7h, &ADC10MEM    ; ADC10MEM = A0 < 1.5?
           JLO     Check0_85V
           JMP     NO_BATT_OR_FULLCHARGE

NO_BATT_OR_FULLCHARGE  bis.b    #01h, &P1DIR
           bis.b    #01h, &P1OUT         ; P1.0 = 1 -> Alarm Status (on)
           jmp     END_ADC10ISR

Check0_85V  cmp      #022Dh, &ADC10MEM    ; 0.85V CHECK
           jhs     Check1_42V
           jmp     precharge_Setup

precharge_Setup
SetupP1_4   bis.b    #010h, &P1DIR         ; P1.4 output
           bis.b    #010h, &P1SEL         ; P1.4
           mov.w    #256, &CCR0          ; PWM Period
SetupC3     mov.w    #OUTMOD_6, &CCTL1    ; CCR1 toggle/set
           mov.w    #128, &CCR1         ; CCR1 PWM Duty Cycle
           mov.w    #TASSEL_2+MC_1, &TACTL ; SMCLK, upmode ;output 0.1c on A1
           jmp     Check0_85V

Check1_42V  cmp.w    #03A3h, &ADC10MEM    ; ADC10MEM = A0 > 1.42V?
           JHS     CheckIsense
           jmp     Constantvoltagecharge1

Constantvoltagecharge1
SetupP1_4_2  bis.b    #010h, &P1DIR         ; P1.4 output
           bis.b    #010h, &P1SEL         ; P1.4
           mov.w    #256, &CCR0          ; PWM Period
SetupC4     mov.w    #OUTMOD_6, &CCTL1    ; CCR1 toggle/set
           mov.w    #128, &CCR1         ; CCR1 PWM Duty Cycle
           mov.w    #TASSEL_2+MC_1, &TACTL ; SMCLK, upmode ;output 0.1c on A1
           jmp     Check1_42V

CheckIsense  cmp      #03B6h, &ADC10MEM    ; A0=1.45V
           jeq     END_ADC10ISR
           jlo     Constantvoltagecharge

Constantvoltagecharge
SetupP1_4_3  bis.b    #010h, &P1DIR         ; P1.4 output
           bis.b    #010h, &P1SEL         ; P1.4
           mov.w    #256, &CCR0          ; PWM Period
SetupC5     mov.w    #OUTMOD_6, &CCTL1    ; CCR1 toggle/set
           mov.w    #128, &CCR1         ; CCR1 PWM Duty Cycle

```

```

SetupC5      mov.w    #256,&CCR0    ; PWM Period
             mov.w    #OUTMOD_6,&CCTL1    ; CCR1 toggle/set
             mov.w    #128,&CCR1    ; CCR1 PWM Duty Cycle
             mov.w    #TASSEL_2+MC_1,&TACTL    ; SMCLK, upmode ;output 0.1c on A1
             jmp     CheckIsense

END_ADC10ISR      reti                ;
;-----
;-----
TERMINATE_CHARGE  CALL TERMINATE
TERMINATE      mov.w    #0000h, &TACCR2    ;stop the timerA
             bic.b    #08h, &P1OUT    ;kill_led

StopADC10      mov.w    #0000h, &TACCRO    ;stop the timer for PWM
             bic.w    #ENC, &ADC10CTL0    ; ADC10 disabled ->FULLstop
             mov.w    #WDTPW+WDTHOLD, &WDTCCTL    ; Stop WDT
             bis.w    #LPM0+GIE, SR    ; LPM0
             RET

;-----
COMMON INTVEC    ; Interrupt Vectors
;-----
ORG    ADC10_VECTOR    ; ADC10 Vector
DW    ADC10_ISR
ORG    RESET_VECTOR    ; POR, ext. Reset
DW    RESET
END

```

Figure 20c Battery charger source code

The ADC10 interrupt service routine is the software constant voltage charge implementation. Basically, the MSP430F2132 is called out of LPM0 and sampling is stopped to check the current value acquired by the ADC10. First we confirm that a battery is connected by confirming that the voltage signal is between 0.3V and 1.5V. If the signal is not within this range then the LED at Port 1.0 is lit.

The next loops are checks of the voltage value on A0 in increasing order from 0.85V to 1.42V to 1.45V. If the voltage check fails, the system puts out a 50% duty cycle pulse width modulated signal on Port 1.1.

Once the interrupt service routine for the ADC10 is complete the mainloop is executed again and the battery condition is checked to verify the battery is not fully charged. If it is, then the terminate routine is jumped to, where the timers and ADC10 are stopped and the PWM signal ceases. The microcontroller is then returned to LPM0.

3.1.1b Sourcecode design, build and test

Figure 22 describes the Sourcecode design process. The control program was designed using a modular design approach in which the different tasks such as pulse width modulation, A/D conversion and timing were completed as modules. Therefore 3 modules were designed and tested. The ADC module was designed first and tested to read the signal from channel A0. This was checked by using an LED on the breadboard, which would light up once a repeated sampling of the channel has been done.

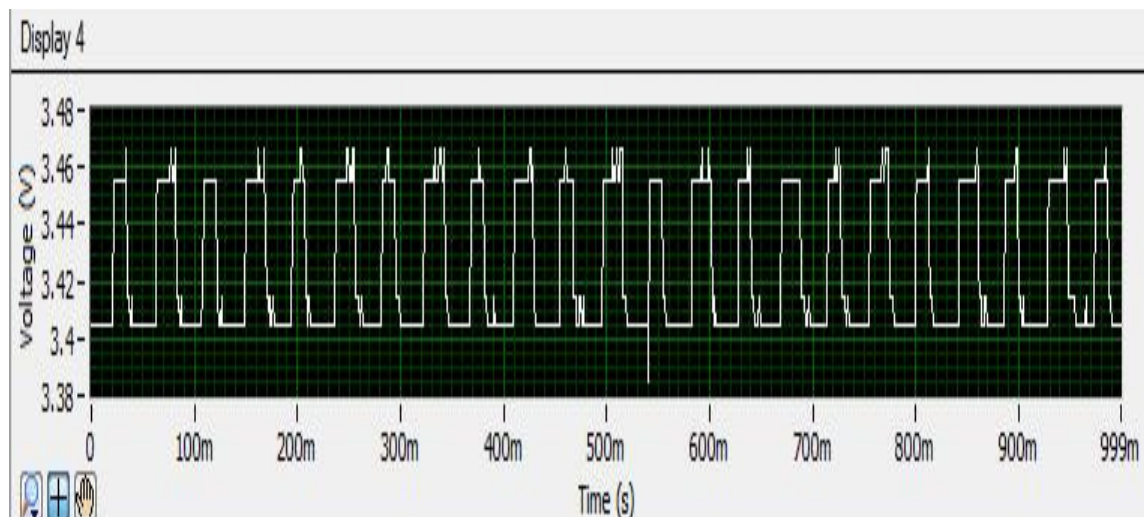


Figure 21 Pulse Width Modulation of Li-Ion battery voltage.

Once, this was done, the pulse width modulation module was designed to act as a switch that turned on and off at Port 1.1. It was tested with an LED and once the LED started blinking, an oscilloscope was used to probe the signal to confirm that a 50% duty cycle signal was being produced. See figure 22, which shows the effect of the PWM signal on the battery voltage. The safe timer was designed to count up to 30 minutes using Timer A as the clocking system with the Master Clock driving the Digital Clocking Oscillator. Finally, the three modules were then integrated and built to create the final program that was tested and deployed for this project.

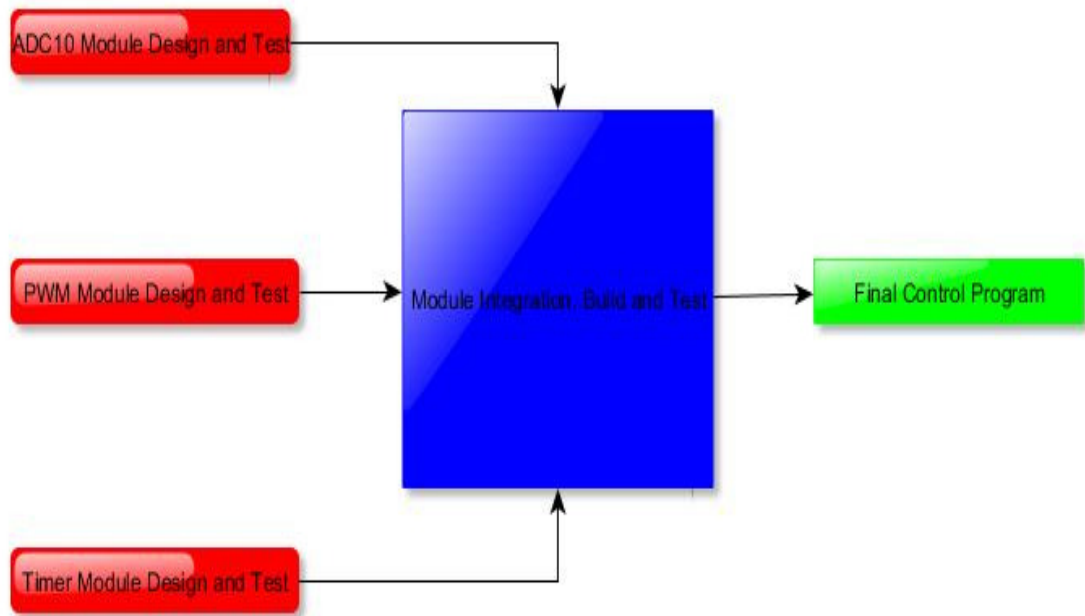


Figure 22 Source Code Modular Design Process

3.2 Full System Integration

After the software was designed, it was tested first with a TT1 EL302D Dual Power Supply Unit, see figure 23. This was necessary to confirm that the system actually could handle a stable DC power source and that the large signal behaviour from the electronic circuit matched the characteristics required, such as the 50% duty cycle signal which was probed by the oscilloscope to ensure that it was actually a pulsed signal that was output at the correct port. Figure 24 shows the digital settings of the Dual Power Supply that were used for the initial test.

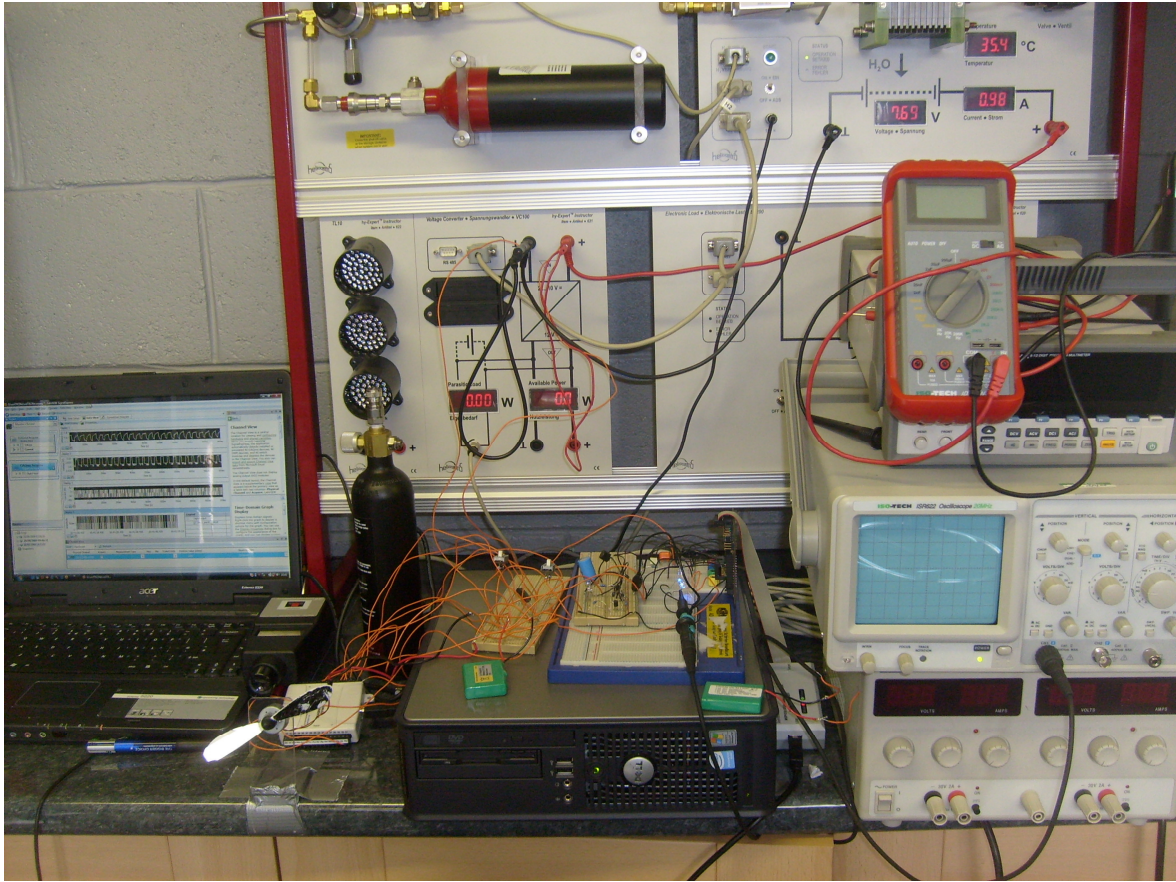


Figure 23 Initial Test Module with Dual Power Supply Unit and Oscilloscope

In figure 24, the test module circuit that was designed is in the middle while 2 different Power supply settings on the left and right show the voltage input to the MSP430F2132 which is 3.7V and the other voltage setting is used to simulate the connection of a 4.2V fully charged battery and a dead battery.

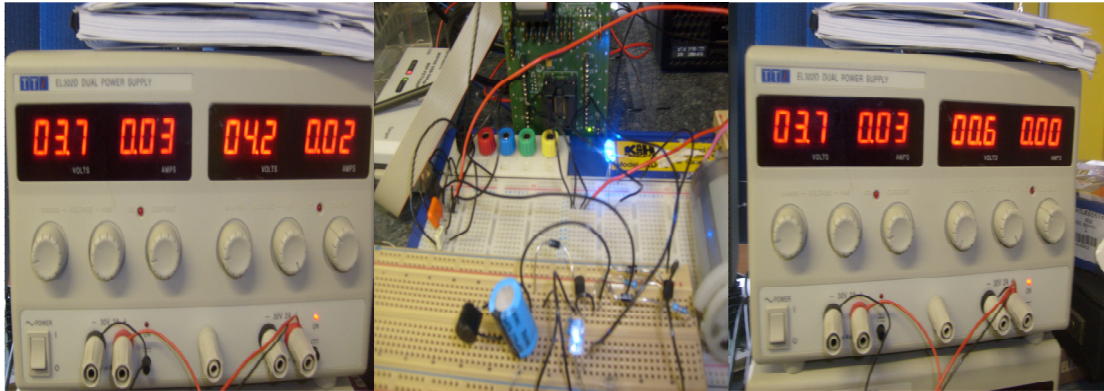


Figure 24. Dual Power Supply and Initial circuitry showing the Power Supply and Pulse width Modulation Test Modules

Please note that the condition photographed is for a live-fully charged battery, that is why the blue LED's are lit.

3.2.2 Integration of Stand Alone System

One objective of the design process is to integrate the system so that it can standalone and not receive power from the Dual Power Supply Unit. This was achieved by connecting the different modules in figure 17b in a serial configuration and including the Data Acquisition Module as shown in figure 25.



Figure 25 Fully Integrated Standalone system

Moving from left to right in figure 25, the blue laptop is the Alienware PC from which the control program was debugged and run. The second laptop runs the Signal Express program for the Data Acquisition endeavour and stores the data on the grey hard drive. The NI USB 6088 is in the middle right behind the DC motor and double blade fan (which has one blade painted black). The Heliocentris FC50 and Hydrogen Supply panel is behind the electronic circuit that contains the power supply regulation system, the pulse width module, the switch gear for the load and the green Varta Li-Ion battery. The Oscilloscope shows a moving stream of the 50% duty cycle signal that charges the battery.

3.3 Drive Cycle Emulation and Motor Load Design

This part of the system was designed to meet the final objective of generating drive cycles. The drive cycle was simulated using a simple switch mechanism and a 1.2ohm

resistor as a load. In figure 26, the switch mechanism consists of two switches, J1 and J2. J1 is used to connect the 10mW DC motor to the Li-Ion battery. When J1 is closed and J2 is open, the fan is energized and the blades begin to turn at maximum speed. When J1 and J2 are closed, the emulator simulates an increase in the load on the system or a steep incline in the real world. This draws more energy from the battery, simulating a sustained increased drainage of the battery's energy.

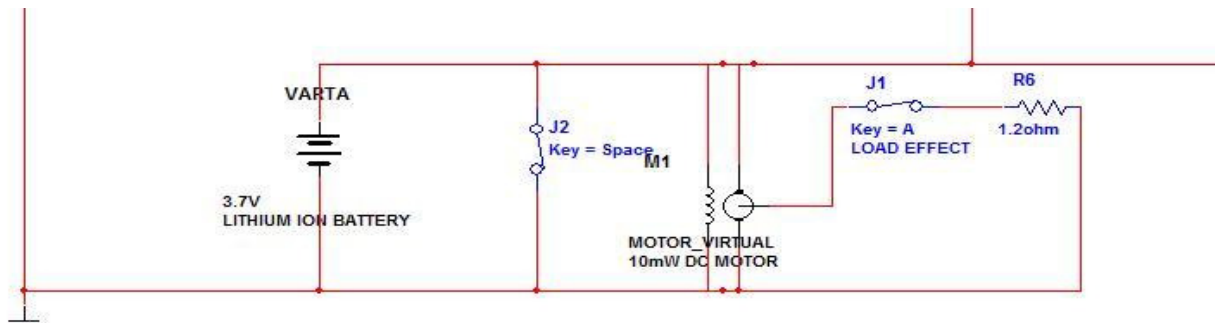


Figure 26 the Drive Cycle Emulator

The Drive Cycles that will be discussed in the next chapter were generated by painting one of the blades on the fan black and using a Tachometer to measure the number of revolutions as the motor powered by a fully charged battery was run for a one hour period. This drive cycle emulates the journey from Stornoway bus stop to Port Ness which is the red route on the map in figure 27 which takes 1 hour to complete by bus over 26.1 miles. In chapter 4, the system will be scaled up and a complete analysis will be done on this drive cycle.



Figure 27 Stornoway-Port Ness Route

4.0 Results and Discussions

4.1 Charge Cycle Analysis

In chapter 2, the constant voltage charging method was mentioned as the chosen method for the battery charger system design. The results in this chapter will demonstrate the efficacy of this method as it was implemented during the experimental procedures that were carried out to test this prototype.

During the constant voltage charge process of the Varta Li-ion batteries, data was collected from the Heliocentris and Varta Li-ion battery using the National Instruments Labview Signal Express and played back. Figure 28 shows the data for the charge cycle that was generated for a fully discharged battery.

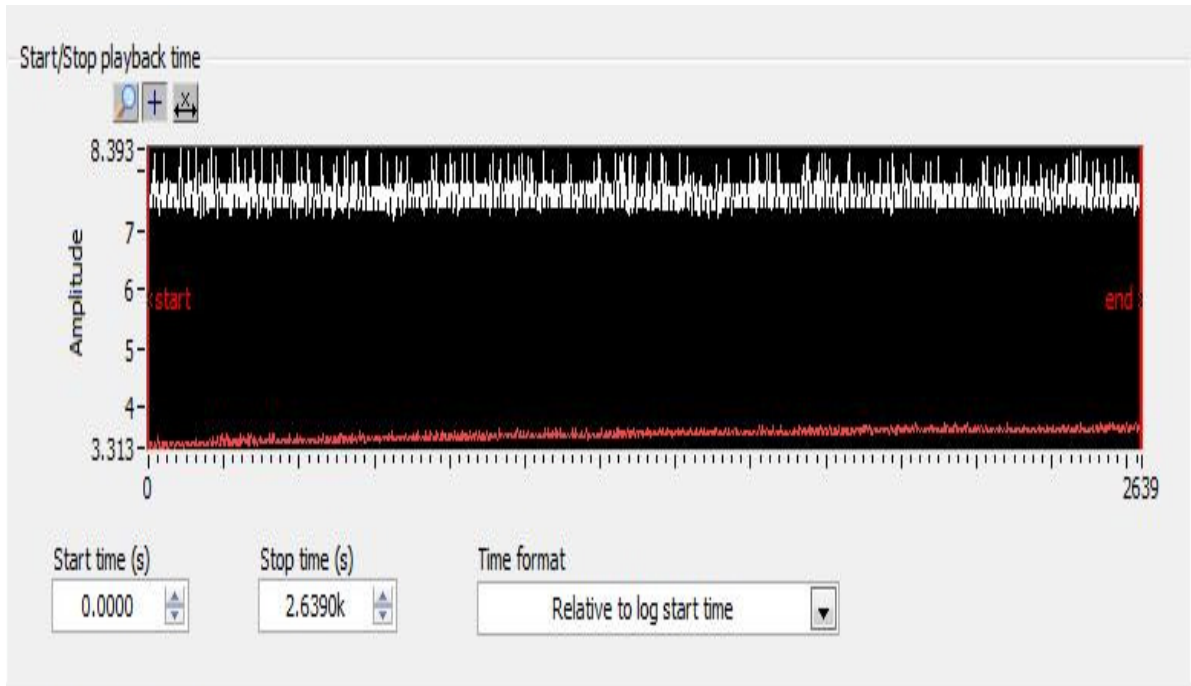


Figure 28 Charge cycle of the battery

In figure 28, the white line is the voltage of the FC50, while the red line represents the voltage of the Li-Ion battery. The y-axis is the voltage axis and the x-axis is the time in seconds. It was observed that the charging process took only 44minutes (i.e. 2639seconds). This exposes the efficacy of the charger that was designed for this system as it employs pulse width modulation to efficiently transfer the power from the FC50 to the Li-ion battery during the charge process. It is important to note that the battery reaches its minimum discharge voltage level at 2.75V (as mentioned in the literature review). At this voltage level the protection circuit kicks in and limits any further discharge. Since the data log was terminated to collect the charge cycle data, this minimum discharge voltage level is only visible in subsequent data logs that will be presented for the discharge cycles generated during this experiment.

Figure 29 is a much higher resolution of the voltage of the Li-Ion battery charged over the 43minute period by the constant voltage process controlled by the MSP430F2132.

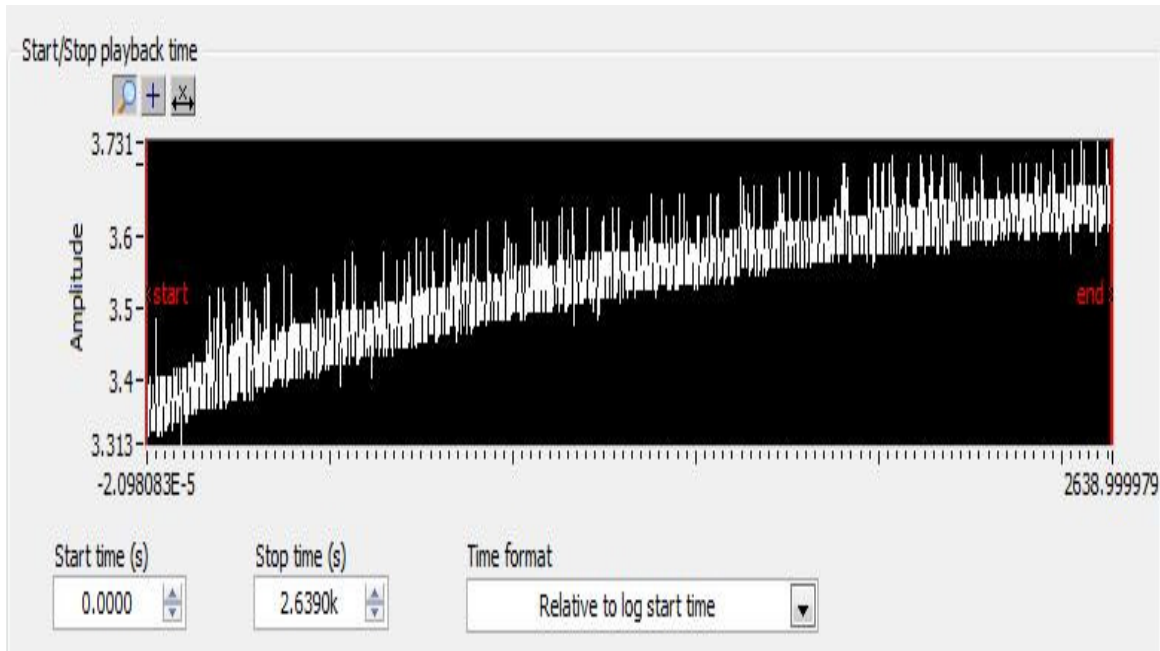


Figure 29 Voltage of the Li-Ion Battery during the constant voltage charge cycle

It was observed from the graph above that the voltage characteristics matched the constant voltage characteristics described in the literature review. This is a very important checkpoint as it validates the battery charger design and efficiency. The battery charges up to its rated voltage, 3.7V. In subsequent sections, the protection circuit kicks in at the maximum overcharge levels and maintains a plateau. The voltage signal might look noisy, this is due to the resolution of the data acquired, which is 1000 samples per second.

The voltage from the FC50 was also monitored on the NI-Labview Signal Express platform. In figure 30, the FC50 supplies a relatively constant voltage and this voltage is maintained throughout the constant voltage charge process. This is another checkpoint as the FC50 voltage profile should remain constant during the charge and discharge cycles of the Li-Ion battery. The average voltage of the FC50 during this process was 7.75V.

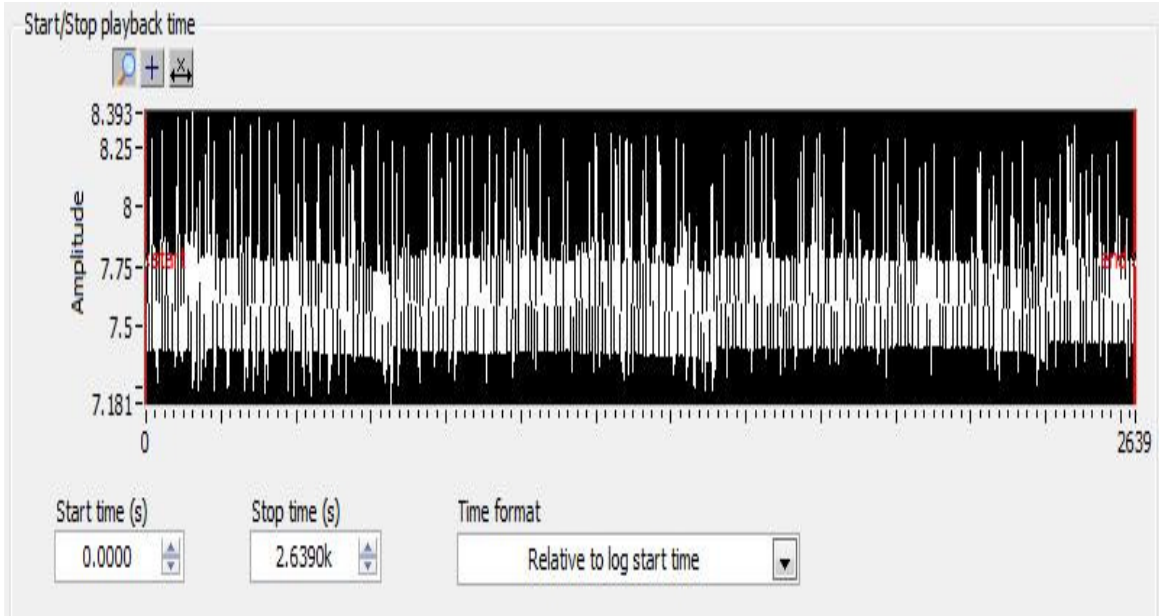


Figure 30 FC 50 voltage data during charge cycle

4.2 Discharge Cycle Analysis

The discharge cycle was generated in tandem with the drive cycles which will be discussed in subsequent sections.

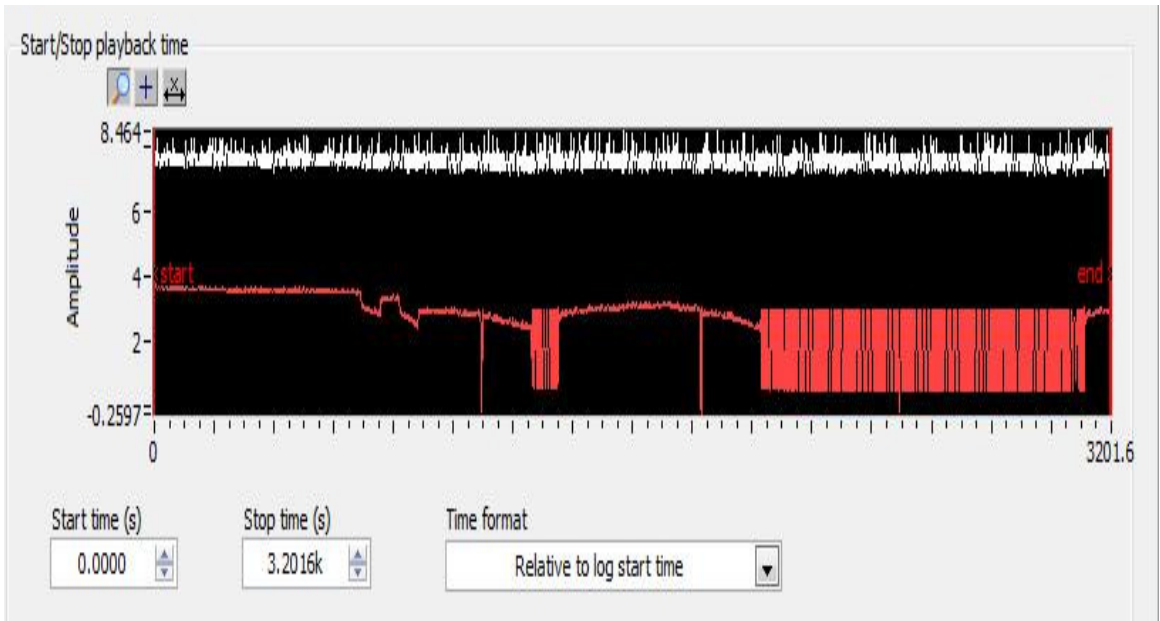


Figure 31 Discharge cycle of the battery showing FC50 and Battery voltages

Discharge of the battery was executed by switching on the 10mW fan to emulate a driven motor and adding a 1.2 ohm resistor to the load to simulate inclines and sloped terrains. In figure 31, the voltage profiles for the FC50 and the Varta battery were acquired via the NI-Labview signal express platform showing the effect of the constant and varied loads on the voltage profile during the drive cycle emulation. The FC50 is the white line, while the battery is the red one.

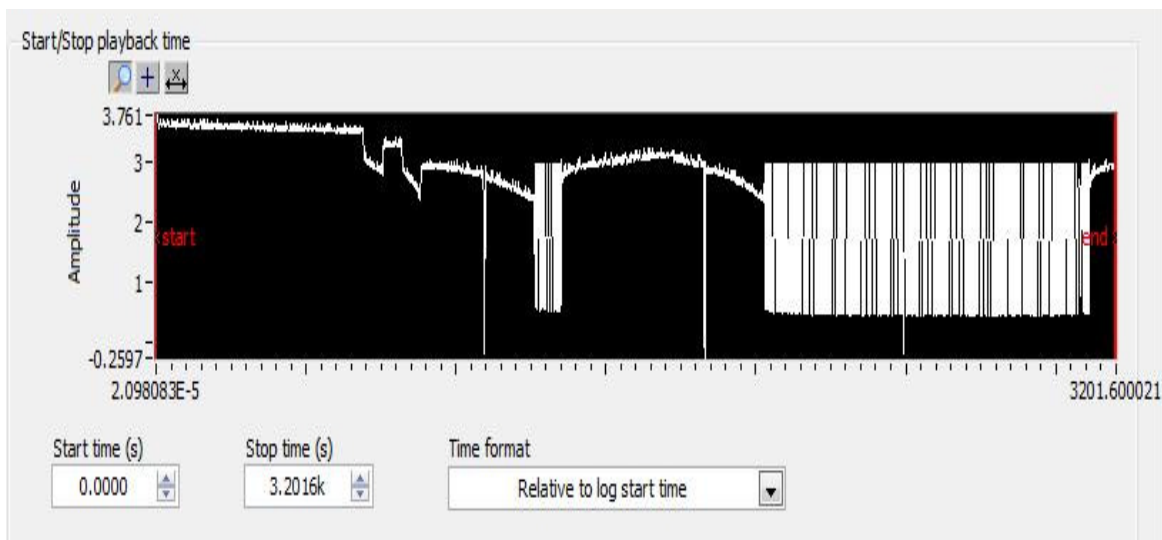


Figure 32 Voltage of the Li-ion battery during charge cycle

The Discharge cycle in figure 32 was generated over a 53 minute period. The y-axis represents the voltage signal, while the x-axis represents the time in seconds. The discharge cycle is a representation of the drive cycle emulated during the project.

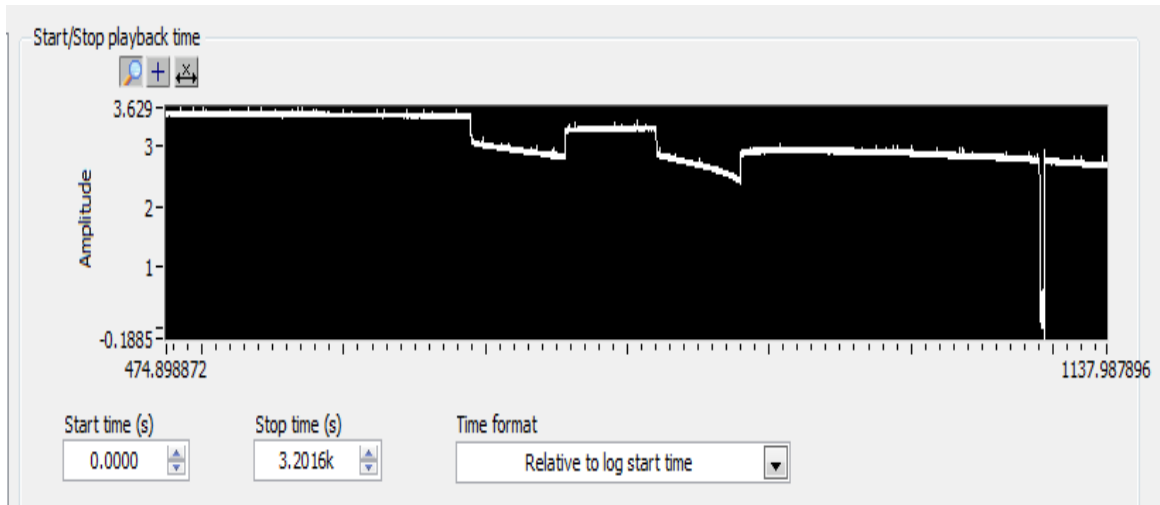


Figure 33 Initial loading of the battery to emulate sloped terrain

The steep voltage drops in figure 33 represent periods during the discharge cycle that emulate a change in the slope of the terrain that would result in an increased load on the battery. As mentioned in the previous chapter, this was accomplished by adding a 300W, 1.2 ohm resistor to the load. The first drop occurs 11.86 minutes into the journey and is sustained for 2 minutes and 2 minutes later the same voltage drop is initiated by switching on the resistor load. As the discharge continues, the battery voltage level passes the minimum over-discharge voltage level in figure 33. This becomes apparent when the load is increased by connecting the resistor. As soon as the load is increased, the motor speed drops severely and the protection circuit module becomes activated.

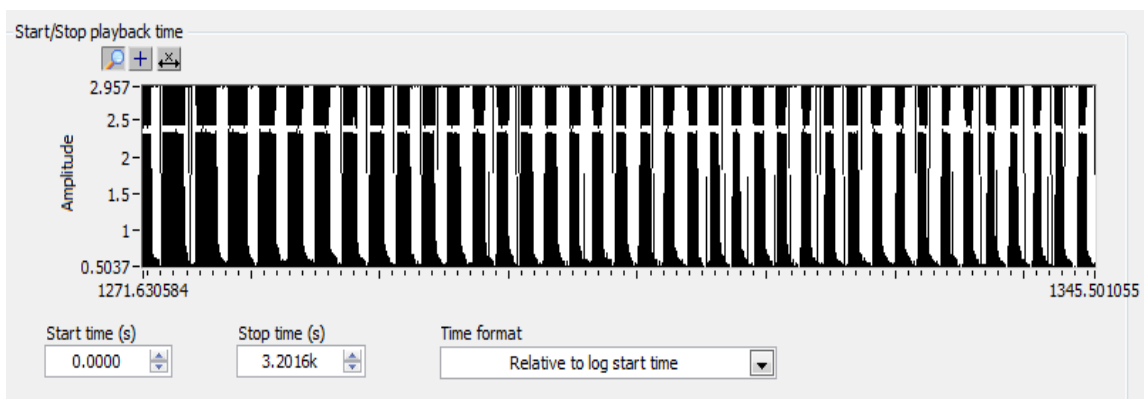


Figure 34 Over-discharge of the battery and protection circuit activation

Any further increase in the load, results in delays of up to 40-200 milliseconds, so that the battery can charge quickly and drive the load. This is evident from the over-discharge after loading the battery with the motor and resistor, in figure 34, the voltage signal oscillates between a minimum of 0.6V and 2.95V. It was observed that the battery's protection circuit takes on some occasions 30.84 milliseconds to recharge back to 2.95V before discharging again to 0.6V. At other times, the protection circuit takes longer, up to 60 milliseconds.

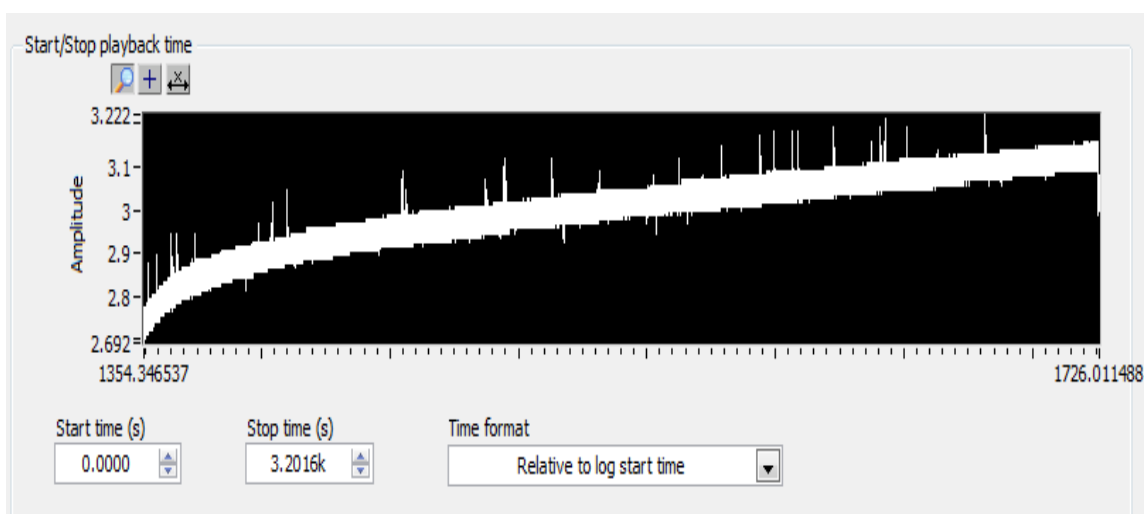


Figure 35 Short Stop and recharge

A 6 minute stop/start was executed to emulate a stop at Bavras which is on the route of the drive cycle that was generated. In figure 35, the battery charged from 2.692V to 3.161V in 6.21 minutes. This means that a short stop to pick up passengers (which is within the 6 minute time window) results in a 17% increase in the state of charge occurred. In a rural region like the Western Isles, where sheep roam the hills and sometimes get on the roads, this could translate to minimum but essential recharge of the battery pack. It was also observed that when the short stop occurred the recharge was instantaneous. This is very important because drive cycle profiles such as urban profiles would allow for quick recharge that will help keep the battery from reaching the minimum over-discharge voltage.

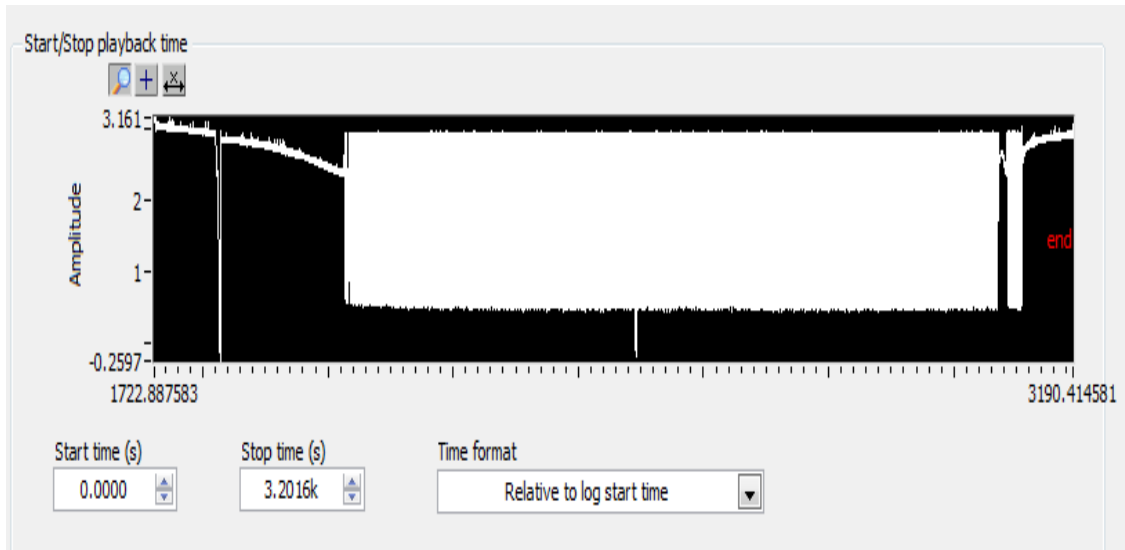


Figure 36 Final discharge and end of drive cycle

In figure 36, right after the short stop at Bavras, as the drive cycle emulation continues there is an emulation of a change in the slope of the terrain. It occurs below the minimum discharge voltage level and the protection circuit becomes activated as is evident from figure 37. The protection circuit causes a delay/resume sequence for the charge and discharge of the battery. In the next subsection, this delay/resume will be discussed in relevance to the motor speed.

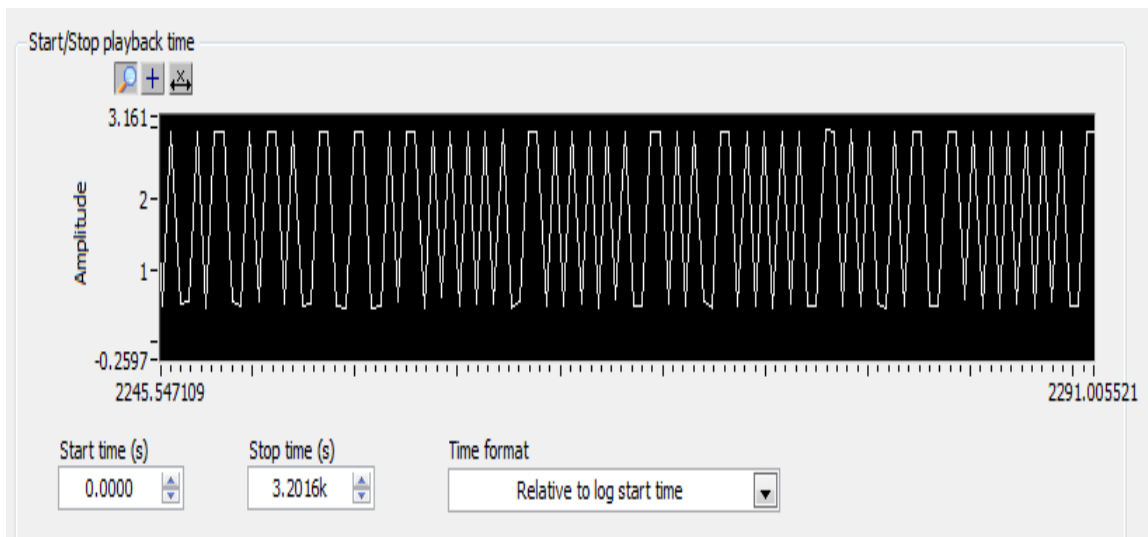


Figure 37 Delay/Resume sequence for final discharge.

4.3 Drive Cycle Analysis

The Drive Cycle emulated for this project is known as a rural drive cycle. This is due to the location in which the drive cycle was generated. Stornoway and the surrounding towns in the Western Isles can be classified as rural with respect to the road and routes for transport vehicles. In figure 38, the red route was emulated in the drive cycle that was generated for this drive cycle.



Figure 38 Western Isles map and red route

To emulate this drive cycle in the lab, the DC motor was run for 1 hour. During this time, changes in the slope of the terrain were emulated at the re-entrant on the map before Bavrass, at Ballantrushal, at Melbost and at North Galson. The rest of the terrain on the map looked flat and a real road trip on that route from Stornoway to Port Ness proved this, as well.

The Drive Cycle generated in figure 39 shows the varying speeds of the motor over a 57 minute period. As the terrain changes, the load on the battery changes; this is evident

from the change in the motor speeds as an additional load of 1.2 ohms is added by engaging the switch on the drive cycle emulator circuit.

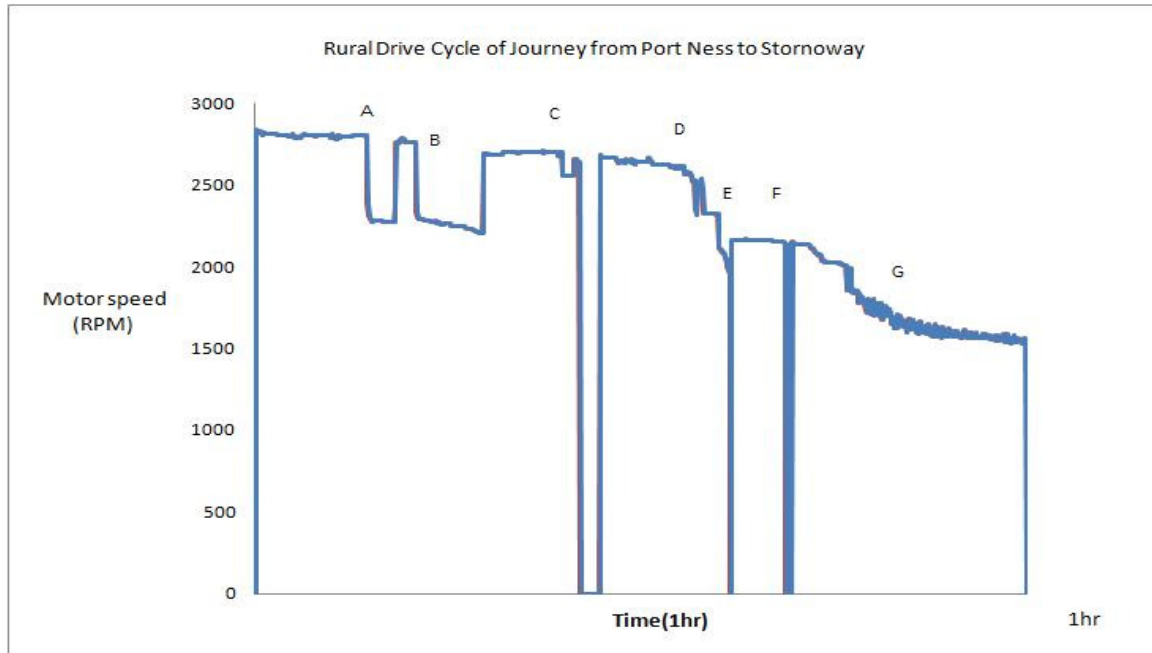


Figure 39 Drive Cycle Emulation for the journey from Port Ness to Stornoway

The Drive cycle above will be compared to the discharge cycle of the battery during the emulation process. It was observed that the speed of the motor decreased at a constant rate from 2836 rpm to 2804 rpm during the first part of the journey to Laxdale. At the re-entrant before Bavras (at point A), an increase in the gradient of the terrain was emulated by connecting the 1.2ohm resistor to the battery while maintaining the connection to the motor. This increase in the load on the battery is evident from the first steep voltage drop in figure 40. The motor speed at this point decreases sharply from 2804 rpm to 2382rpm.

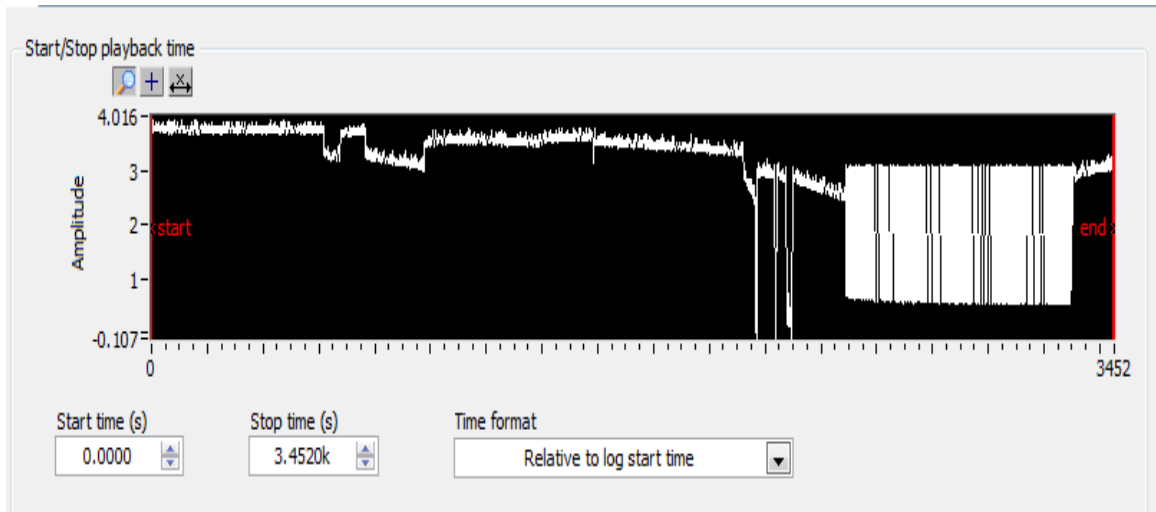


Figure 40 Discharge cycle of battery during Drive Cycle emulation shown in figure 39

A change back to flat terrain is emulated and another change back to a steep slope is sustained for 3.71minutes. This results in another decrease in the motor speed in figure 39, from 2765rpm to 2331rpm. A voltage drop of 3.75V to 3.5V occurs as the load on the battery is sustained, discharging the battery to the 3V level.

At Bavras, the motor is stopped and the battery is allowed to charge for 3 minutes. This is the region below the C mark, where the motor speed goes to zero. The battery is observed to charge from 3.45V to 3.75V as shown in figure 41.

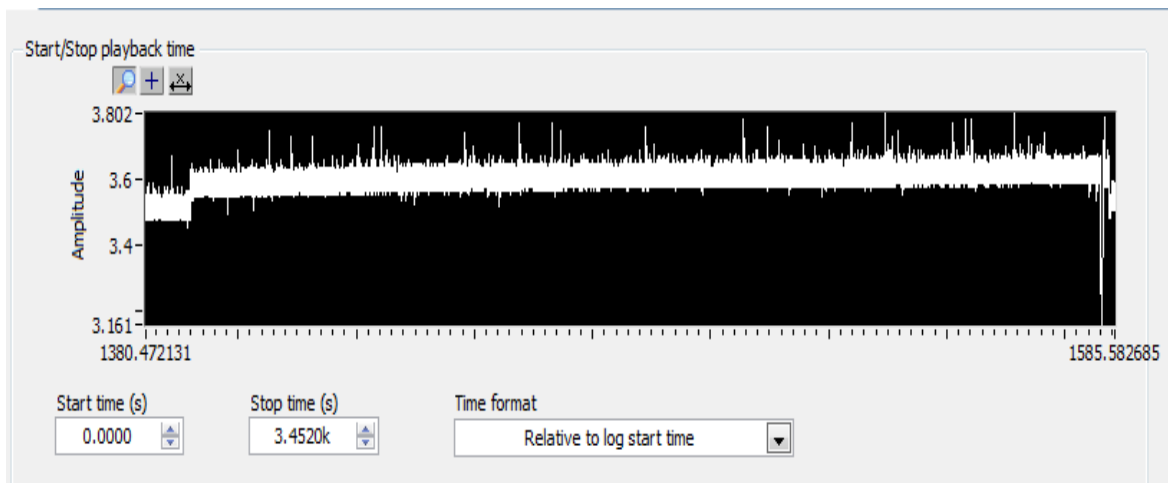


Figure 41.Short Stop at Bavras (region C of drive cycle)

After the short stop the battery is loaded with the motor only. There is a sudden drop in the voltage from 3.75 to 3.161 volts, this is as a result of the starting torque of the motor which is highest as the motor transitions from static to dynamic states. The voltage is stabilized at 3.47V as the counter electromotive force in the armature and the battery voltage gradually equalize. It must be noted that this never happens, as the motor current will be zero and the speed will become zero as well. At the moment the load torque equals the torque generated by the armature current in the motor, the voltage stabilizes at the 3.47V level.

At region D, a quick increase in the load is made, leading to a discharge to 0V, in figure 40. It is observed that the protection circuit does not get activated. More changes in the slope of the terrain are emulated for in regions E and F and the battery is discharged to zero volts, both times.

As the battery discharges below the minimum over-discharge level at 2.75V, the protection circuit gets activated. In region G, the slope of the curve gradually approaches infinity as a constant delay/resume sequence of charge and discharge occur. As the speed of the motor falls below 2000 rpm, the motor speed oscillates with the voltage of the battery as the protection circuit initiates this delay/resume sequence to prevent a full over-discharge of the battery.

4.4 DC Motor Characteristics during Drive Cycle Emulation

The Mechanical Power, Torque and Efficiency were evaluated during the drive cycle emulation.

Due to the fact that a small 10mW motor was deployed for this project, an assumption was made to the effect that all IR losses were negligible as they would be very small compared to the supply voltage.

This allowed the use of the supply voltage (E_s) for the calculation of the mechanical power, by equating it to the armature voltage (E_o).

Therefore, mechanical power = $(E_s) I$

For this system the power curve will track the voltage curve of the discharge cycle in figure 40. From Figure 42, which is the current that passes through a 1.2ohm resistor in the drive cycle emulator. The maximum power dissipated when the switch is closed is 8.26W.

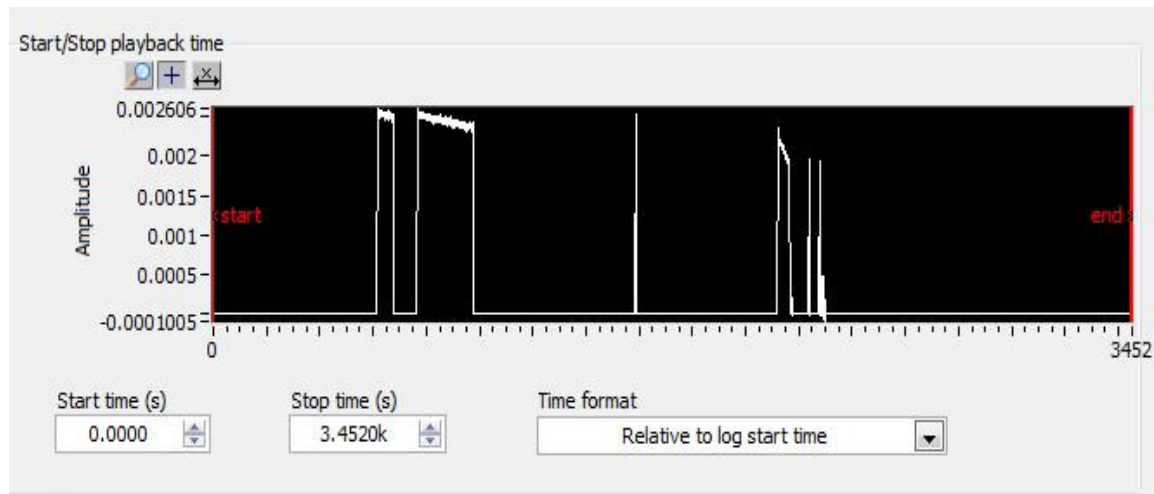


Figure 42 Current data for 1.2ohm resistor (current values were divided by 1000)

The Torque will also track the same curve in figure 40, with the minimum torque of 0.03N.m occurring at the lowest speed of 1532 rpm and the maximum torque of 0.038N.m occurring at the highest speed of 2836rpm. This is consistent with known DC motor principles, as a higher torque must turn the motor's shaft from a stationary position until the torque from the load and the motor become equal.

The electrical efficiency of the system is a product of all three components of the hybrid drive system. The FC50 supplied a maximum power of 50W over the course of the discharge cycle in figure 31. At its peak, the efficiency of the FC50 is 63%. The Varta batteries supplied a maximum power of 8.26W to the DC motor (during emulation of sloped terrain). The system efficiency at maximum operation is very low. This is as a result of poor sizing of the system load. The system efficiency as a product of the hybridized energy sources is 10.4 %.

5.0 Conclusions and Recommendations

5.1 Conclusions

Based on the results acquired during the course of this project, the hybrid serial drive system can be effectively deployed with a Fuel cell as the primary energy source and a Lithium Ion Battery as the secondary energy source while the MSP430F2132 microcontroller efficiently dispatches power to the battery as it drives a motor.

One major achievement was the deployment of the battery charger, which was designed from scratch in the labs and programmed to be controlled by the MSP430F2132. It took less than 1 hour to charge a fully discharged battery to its rated voltage of 3.7V.

Another key achievement was the ability to sustain a constant energy drive from the fuel cell, enabling it to charge the battery only and not deliver power directly to the primary load. It is evident from the results that as long as the primary energy source (i.e. the fuel cell) does not expire, the secondary energy source (i.e. the lithium ion battery) can drive the motor. This is made possible by the employment of the constant voltage charge method in the charge algorithm utilised by the MSP430F2132, which delivers a pulse width modulated signal from the hardware to enable effective dispatch of power to the battery. The constant voltage charge method was very effective and is the easiest method for keeping the battery charged over the drive cycle emulated. A 17% increase in the state of charge was observed over a 6 minute period during a short stop. In an urban setting this could guarantee availability of battery power as there are more starts and stops in the city, which would translate to more short periods for recharging the battery.

The Protection Circuit Module (PCM) is a very important component of the Lithium-ion battery. This is where they surpass the Nickel Cadmium and Lead Acid solutions because, the PCM helps to maintain the state of charge around 75%. This was very essential for this prototype, because the motor kept running even when the voltage dipped close to the 0V level. The PCM always initiated a delay/resume sequence of

approximately 50 milliseconds to enable a temporary charge and discharge of the battery, even though the motor speeds oscillated with this sequence. However, no extra loading of the system could be done as it would result in a full stop of the motor.

Finally, it was concluded that appropriate sizing of system components would result in a more efficient hybrid. If the system was scaled up linearly while maintaining the same materials, the efficiency will increase and so will the energy density. However, an increase in size will also result in an increase in the surface area as well as the temperature of the working system. This means more will have to be done to cool the system effectively.

5.2 Limitations

The system was limited by the lack of a working crystal oscillator. This would have ensured better pulse width modulation at a higher frequency, enabling the constant charge process to occur faster and much more efficiently.

There was also a lack of proper sized motors. A 10mW motor was used for this project.

5.3. Recommendations

An increase in the scale of the prototype for future designs is very profitable as larger loads can be driven and the system could be ported to a transport vehicle. If this is done, the design goal should be to drive 4 separate motors powered by the battery while it is charged by the fuel cell. A better control algorithm should be deployed, to control the dispatch of energy from the battery.

A second or third array of lithium-ion batteries can be deployed while using a load dispatch system controlled by the MSP430F2132 to guarantee an operating reserve. This operating reserve will prevent the activation of the PCM, enabling a smoother discharge and drive cycle. Stationary applications are also a possibility, as the system has a battery

charge incorporated to it. If an alternator is incorporated to the system, then it could keep one array of batteries charged, while another array drives the primary load.

Research into speed control and efficiency optimisation is very necessary as the speed control component of this project is very rudimentary.

Regenerative Braking is also a major avenue for research, as the start/stops can generate reactive power which can be captured by electric dual layer capacitors or super-capacitors. The use of flywheels can also be investigated in the effort to maximise efficiency and improve the energy storage potential of the drive system.

References

- [1] Brent Crude Oil Prices www.thisismoney.co.uk
- [2] A Crude Awakening-The Oil Crash (Produced and Directed by Basil Gelpke and Ray McCormack in 2006)
- [3] PEM fuel cell diagram <http://www1.eere.energy.gov/hydrogenandfuelcells/>
- [4] PEM fuel cell http://www1.eere.energy.gov/hydrogenandfuelcells/fuelcells/fc_types.html#pem
- [5] Heliocentris Instructor http://www.heliocentris.com/fileadmin/user_upload/Datenbl%C3%A4tter/EDU_TD_Instructor_INT_eng_0907_web.pdf
- [6] The battery university, Isidor Buchmann, founder and CEO of Cadex Electronics Inc., in Vancouver BC. <http://www.batteryuniversity.com/partone.htm>
- [7] Texas Instruments Lithium-Ion Battery Charger Solution <http://focus.ti.com/lit/an/slaa287/slaa287.pdf>
- Automobile Electrical and Electronic Systems, Tom Denton, third edition, 2007
- [8] Rechargeable Lithium Batteries:Li-Ion Technology Dr. Martin G. Hake et al, VARTA Special Report 1/1996
- [9] Electric and Hybrid Vehicles: Advanced Nickel-Metal-Hydride and Lithium-Ion Batteries Uwe Köhler, Franz J. Kruger, Jörg Kämpers, Matthias Maul, Eberhard Niggemann VARTA Special Report 3/1997
- [10] Varta Lithium Ion Battery Design, <http://docs-europe.electrocomponents.com/webdocs/0ac9/0900766b80ac9773.pdf>
- [11] Electric Machines, Drives and Power Systems, Theodore Wildi, Fifth Edition, 2002
- [12] Selection of Electric Motor Drives,for Electric Vehicles X. D. Xue, K. W. E. Cheng, and N. C. Cheung,Department of Electrical Engineering, the Hong Kong Polytechnic University,Hung Hom, Kowloon, Hong Kong, China
- [13] Global Modelling of Different Vehicles, Keyu Chen, Alain Bouscayrol, Alain Berthon, Philippe Delarue,Daniel Hissel, and Rochdi Trigui

[14] Future Fuels, Energy Institute, September 2009

[15] MSP430 Users guide <http://focus.ti.com/lit/ug/slau049f/slau049f.pdf>